

Stability of lubricated viscous gravity currents. Part 1: Internal and frontal analyses and stabilisation by horizontal shear

Katarzyna N. Kowal^{1,2†} and M. Grae Worster^{1,2}

¹Department of Applied Mathematics and Theoretical Physics, University of Cambridge, Wilberforce Road, Cambridge, CB3 0WA, United Kingdom

²Trinity College, University of Cambridge, Cambridge, CB2 1TQ, United Kingdom

(Received xx; revised xx; accepted xx)

A novel viscous fingering instability, involving a less viscous fluid intruding underneath a current of more viscous fluid, was recently observed in the experiments of Kowal & Worster (2015). We examine the origin of the instability by asking whether the instability is an internal instability, arising from internal dynamics; or a frontal instability, arising from viscous intrusion. We find it is the latter and characterise the instability criterion in terms of viscosity difference or, equivalently, the jump in *hydrostatic* pressure gradient at the intrusion front. The mechanism of this instability is similar to, but contrasts with, the Saffman-Taylor instability, which occurs as a result of a jump in *dynamic* pressure gradient across the intrusion front. We focus on the limit in which the two viscous fluids are of equal density, in which a frontal singularity, arising at the intrusion, or lubrication, front, becomes a jump discontinuity, and perform a local analysis in an inner region near the lubrication front, which we match asymptotically to the far field. We also investigate the large-wavenumber stabilization by transverse shear stresses in two dynamical regimes: a regime in which the wavelength of the perturbations is much smaller than the thickness of both layers of fluid, in which case the flow of the perturbations is resisted dominantly by horizontal shear stresses, and an intermediate regime, in which both vertical and horizontal shear stresses are important.

Key words:

1. Introduction

The series of experiments described in Kowal & Worster (2015) involving two superposed currents of viscous fluids of different viscosity flowing radially outwards revealed a novel cross-flow fingering instability when the lower layer is less viscous. A sample sequence of photographs of the fingering instability is shown in Figure 1. The instability occurs at late stages of the experiments, causing lobes of highly lubricated, thin regions of high viscosity fluid to advance ahead of less mobile, thicker regions of high viscosity fluid. Despite its characteristically different formation mechanism, there are similarities between the instability observed in the experiments of Kowal & Worster (2015) and the well known Saffman-Taylor instability, involving the intrusion of a less viscous fluid into a more viscous fluid in a porous medium (Saffman & Taylor 1958) or Hele-Shaw cell.

† Email address for correspondence: k.kowal@damtp.cam.ac.uk

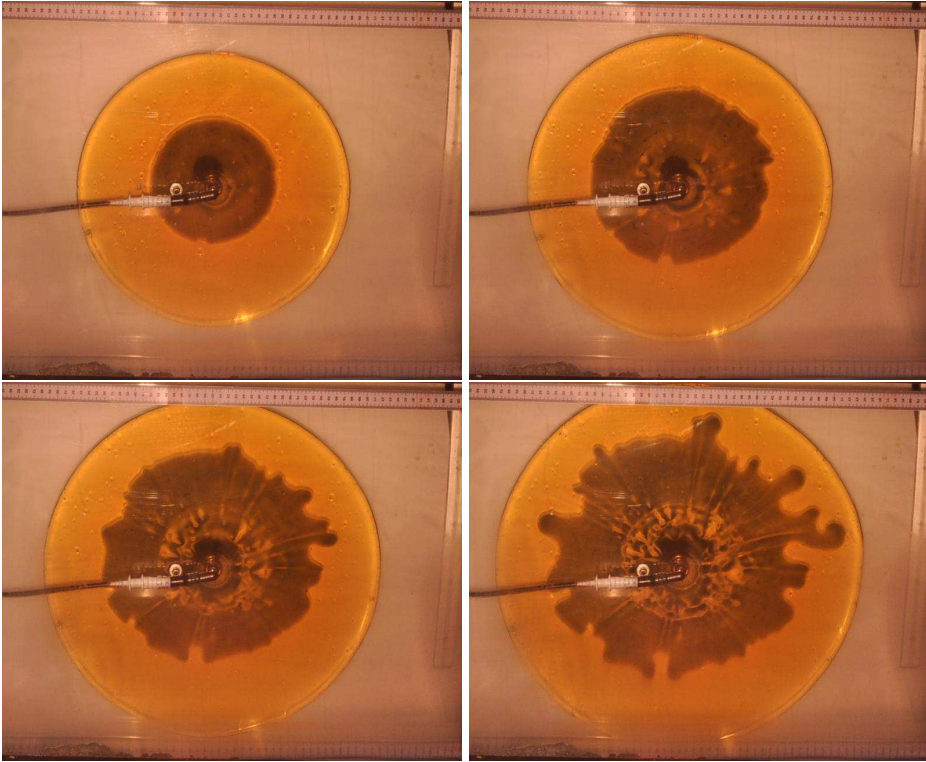


Figure 1: Photographs of the bottom view of one of our experiments $t = 100, 200, 300, 400$ seconds after injection of the lubricant. Less viscous fluid (dye potassium carbonate solution) intrudes underneath a more viscous fluid (golden syrup).

Viscous fingering is ubiquitous in nature and industry and may result in complex, highly branched structures (Saffman & Taylor 1958; Paterson 1981; Homsy 1987; Chen 1989; Thome *et al.* 1989; Manickam & Homsy 1993). Similar phenomena are prevalent in various scenarios, such as in oil recovery processes (Orr & Taber 1984), carbon sequestration (Cinar *et al.* 2009), coating applications and ribbing (Taylor 1963; Reinelt 1995), and morphological instabilities in crystal growth (Mullins & Sekerka 1964). The patterns that emerge may be controlled by varying the injection rate of the less viscous fluid (Li *et al.* 2009; Dias & Miranda 2010; Dias *et al.* 2012), changing the geometry (Nase *et al.* 2011; Al-Housseiny *et al.* 2012; Juel 2012; Dias & Miranda 2013) and elasticity (Pihler-Puzovic *et al.* 2012, 2013, 2014) of the medium, by the use of anisotropy (Ben-Jacob *et al.* 1985), and the use of non-Newtonian fluids (Kondic *et al.* 1998; Fast *et al.* 2001; Kagei *et al.* 2005).

These frontal instabilities can be contrasted with the internal instabilities that arise between co-flowing, superposed viscous fluids. It has been found by Yih (1967), for example, that a contrast in the viscosities of two superposed fluid films between two horizontal plates can cause long-wavelength instabilities and lead to the formation of wavy patterns. This became commonly known for affecting the quality of manufactured products in industrial processes and attracted a breadth of research on the subject, focusing on flows in two spatial dimensions (Kao 1968; Wang *et al.* 1978; Hinch 1984; Hooper & Grimshaw 1985; Hooper & Boyd 1983, 1987; Renardy 1987; Hooper 1989; Chen 1993; Tilley *et al.* 1994; Balmforth *et al.* 2003). Loewenherz *et al.* (1989) and Loewenherz

& Lawrence (1989) later related these results in a glaciological context to the formation of transverse ridges on rock glaciers. The above-mentioned studies of instabilities due to a viscosity difference between two superposed fluid films are all due to an internal instability mechanism and do not involve the cross-flow dimension. The resulting instabilities are longitudinal, in contrast to the fingering patterns observed in the experiments of Kowal & Worster (2015).

The experiments of Kowal & Worster (2015) were motivated by considerations of subglacial till, or water-saturated subglacial sediment, which lubricates the underside of glacial ice sheets, such as those of Greenland and Antarctica, in an idealised experimental setting that aids flow delivery. The part of the experiments relevant to the glaciological setting are their internal dynamics, particularly the viscous coupling between the two layers, rather than their frontal dynamics, at the intrusion front, and it is of interest to determine which of these give rise to the instabilities. In particular, can the instabilities give insight into the formation of ice streams, or regions of ice that are much faster flowing than their surroundings? Their formation has been suggested to result from a spontaneous instability of ice flow through a positive feedback between sliding velocity and basal-melt production (Fowler & Johnson 1995, 1996; Sayag & Tziperman 2008), a triple-valued sliding law (Sayag & Tziperman 2009; Kyrke-Smith *et al.* 2014), or thermoviscous fingering (Payne & Dongelmans 1997; Hindmarsh 2004, 2006). The last of these has also been seen in the context of the surface cooling of viscoplastic lava domes (Balmforth & Craster 2000).

In this paper, we analyse the origins of the instability by posing questions on what the possible instability mechanisms might be and formulating simpler problems that specifically isolate each mechanism. Two main questions arise: is the instability an internal instability, arising from internal dynamics; or is it a frontal instability, arising from viscous intrusion?

To answer the first question, we consider a problem in which both fluids drain off the edge of a finite plate, as shown in figure 2a. This setting allows us to focus on internal dynamics while frontal dynamics play no role. The nature of the problem allows for a clean proof that all normal mode disturbances for any parameter values have negative growth rates. This proves stability for all parameter values and suggests that the experimentally observed instabilities are frontal instabilities. We present the proof in §3 after introducing the governing equations in §2. The mechanism of instability is revealed first in §4 (specifically in §4.1) by considering frontal dynamics, and then modified in §5 and §6.

To examine frontal dynamics, we focus the remaining sections of this paper on a stability analysis in the neighbourhood of the lubrication front, where the instability originates. In §4, we focus on a singular limit in which the densities of the two layers are equal. As a consequence, the order of the governing equations reduces by one and the frontal singularity, which occurs at the tip of the intruding current only when there is a density difference between the layers, reduces to a frontal jump discontinuity (Kowal & Worster 2015). This allows for a local linear approximation to the surface slopes of both layers in the inner region near the lubrication front. In this setup, we characterise conditions under which the flow is unstable and identify the underlying instability mechanism. We find that although the physics of this problem reveals the mechanism of instability, it does not yield a stabilising mechanism for wavelength selection.

We devote the remaining part of this paper to explore the effect of transverse shear as a possible large-wavenumber stabilising mechanism in two dynamical regimes and develop a thin-film theory in each of these. The first regime, described in §5, is one in which the wavelength of the perturbations is much smaller than the thickness of both layers

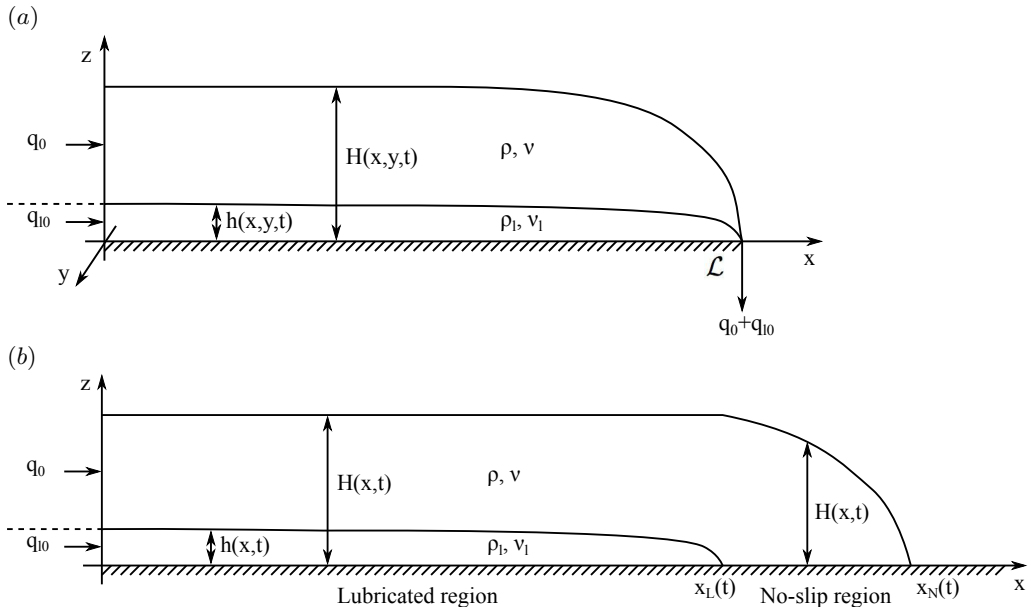


Figure 2: Schematic of two superposed thin films of viscous fluid spreading horizontally under gravity on a rigid horizontal surface with, (a), and without, (b), drainage at $x = \mathcal{L}$ off the edge of the rigid plate. Panel (a) displays thin films of fluid spreading over a finite plate in steady state, whereas panel (b) displays a spreading current with an internal lubrication front. Panel (b) is reproduced from Kowal & Worster (2015).

of fluid, in which case the flow of the perturbations is resisted dominantly by horizontal shear stresses. These stabilize small wavelengths. The physical ideas of §4 and §5 are combined in §6 to determine wavelength selection at intermediate wavenumbers. This final regime is an intermediate regime accounting for both vertical and horizontal shear stresses. We note that this is an idealised scenario, in which only vertical and horizontal shear stresses appear, and the purpose is to determine whether or not these are sufficient to provide stabilisation at large wavenumbers. However, we also note that extensional stress gradients may also become important at similar length scales, prompting the need for a solution to the full Stokes equations near the intrusion front, which we do not attempt in this paper.

We perform a more detailed analysis of the full problem, in which the densities of the two layers are not assumed equal and without the use of local spatial and frozen-time approximations, in the companion paper Kowal & Worster (2018). The companion paper can be read alone, without absorbing all the details of the current paper.

2. Governing equations for lubricated currents

In the present paper, we adopt a two-dimensional geometry for the basic states that we consider. The experiments of Kowal & Worster (2015) were carried out in an initially axisymmetric geometry and the companion paper analyzes the stability for an axisymmetric basic state. We find in the companion paper that the mechanism of instability and the conditions of the onset of instability are unaffected by the change in geometry.

The following is based on the PhD Thesis by Kowal (2016). The systems we analyse are

illustrated in figure 2. The lubricated region in each case consists of two superposed layers of fluid spreading horizontally under their own weight over a rigid plate. We denote the height of the interface between the two fluids by $h(x, y, t)$ and the upper surface height by $H(x, y, t)$. The fluids are of different dynamic viscosities, μ and μ_l , kinematic viscosities, ν and ν_l , densities ρ and $\rho_l (\geq \rho)$, and are released at fixed source fluxes q_0 and q_{l0} , where the subscript l refers to the lower layer. The gravitational constant is denoted by g . Three important dimensionless parameters arise, including the dynamic viscosity ratio, the dimensionless density difference and the flux ratio between the two fluids, given by

$$\mathcal{M} = \frac{\mu}{\mu_l}, \quad \mathcal{D} = \frac{\rho_l - \rho}{\rho}, \quad \text{and} \quad \mathcal{Q} = \frac{q_{l0}}{q_0}, \quad (2.1)$$

respectively. Although the following applies for viscous fluids with general viscosity ratios, we are principally interested in the case in which the lower layer is less viscous, lubricating the overlying highly viscous current.

The dynamics of the underlying current are dominated by vertical shear stresses arising from traction along the rigid plate. However, shear and extensional stress can both play a role within the overlying current. As in Kowal & Worster (2015), we consider the limit in which vertical shear provides the dominant resistance to the flow in both layers. We assume that inertia and the effects of mixing and surface tension at the interface between the layers are negligible and consider a balance between viscous and buoyancy forces. We assume that the films are much thinner than their extent, $\mathcal{H} \ll \mathcal{L}$, where \mathcal{H} and \mathcal{L} are the characteristic thickness and length of the flow, and apply the approximations of lubrication theory.

We apply the following non-dimensionalisation throughout:

$$x = \mathcal{L}\tilde{x}, \quad (H, h) = \mathcal{H}(\tilde{H}, \tilde{h}), \quad t = \mathcal{T}\tilde{t}, \quad (\mathbf{q}, \mathbf{q}_l) = q_0(\tilde{\mathbf{q}}, \tilde{\mathbf{q}}_l) \quad (2.2)$$

where

$$\mathcal{H} = \left(\frac{\nu q_0 \mathcal{L}}{g} \right)^{1/4} \quad \text{and} \quad \mathcal{T} = \left(\frac{\nu \mathcal{L}^5}{g q_0^3} \right)^{1/4} \quad (2.3)$$

are the characteristic thickness and time scales of the currents associated with a length scale \mathcal{L} , which depends on the problem in question and will be specified in the appropriate sections. We drop tildes henceforth.

The horizontal fluid velocities satisfy

$$\mu \mathbf{u}_{zz} = \nabla p \quad \text{for} \quad h \leq z \leq H, \quad \mu_l \mathbf{u}_{lzz} = \nabla p_l \quad \text{for} \quad 0 \leq z \leq h, \quad (2.4a, b)$$

where ∇ is the horizontal component of the gradient operator, and the pressures are given by

$$p = (H - z) \quad \text{for} \quad h \leq z \leq H, \quad (2.5)$$

$$p_l = (H - h) + \frac{\rho_l}{\rho}(h - z) \quad \text{for} \quad 0 \leq z \leq h. \quad (2.6)$$

These are subject to no slip at the base, no stress at the upper, free surface,

$$\mathbf{u}_l = 0 \quad (z = 0), \quad \mu \mathbf{u}_z = 0 \quad (z = H), \quad (2.7a, b)$$

and continuity of velocity and shear stress between the layers,

$$\mathbf{u}_l = \mathbf{u}, \quad \mu_l \mathbf{u}_{lz} = \mu \mathbf{u}_z \quad (z = h). \quad (2.8a, b)$$

These equations can be solved and integrated to obtain the volume flux of fluid, per

unit width, in the lower and upper films,

$$\mathbf{q}_l = \int_0^h \mathbf{u}_l dz = - \left[\frac{\mathcal{M}}{3} h^3 (\mathcal{D}\nabla h + \nabla H) + \frac{1}{2} \mathcal{M} h^2 (H - h) \nabla H \right], \quad (2.9)$$

$$\mathbf{q} = \int_h^H \mathbf{u} dz = - \left[\frac{1}{3} (H - h)^3 \nabla H + \frac{1}{2} \mathcal{M} h^2 (H - h) (\mathcal{D}\nabla h + \nabla H) + \mathcal{M} h (H - h)^2 \nabla H \right]. \quad (2.10)$$

In each film, there are Poiseuille-like contributions from the spreading of each film under its own weight, and Couette-like contributions arising from boundary motion (Kowal & Worster 2015). These are supplemented by mass conservation equations for the two layers,

$$\frac{\partial h}{\partial t} = -\nabla \cdot \mathbf{q}_l, \quad \frac{\partial (H - h)}{\partial t} = -\nabla \cdot \mathbf{q}. \quad (2.11 a, b)$$

and source flux boundary conditions

$$\mathbf{q}_l = \mathcal{Q} \mathbf{e}_x, \quad \mathbf{q} = \mathbf{e}_x \quad (x = 0). \quad (2.12 a, b)$$

The remaining boundary conditions depend on the problem in question and will be discussed as they arise.

3. Internal dynamics: lubricated currents with drainage

Consider two superposed layers of fluid spreading horizontally and steadily under their own weight over a rigid plate of finite length L as depicted in Figure 2a. For the non-dimensionalisation (2.2), we take $\mathcal{L} = L$ in this section. Both fluids are pinned at the singular drainage front, that is,

$$h = 0, \quad H = 0 \quad (x = 1). \quad (3.1 a, b)$$

3.1. Steady solution

The mass conservation equations admit steady solutions that satisfy

$$\mathbf{q}_l = \mathcal{Q} \mathbf{e}_x, \quad \mathbf{q} = \mathbf{e}_x, \quad (3.0 a, b)$$

along with (3.1). These equations can be solved analytically to yield the two-dimensional steady solutions

$$(H_s, h_s) = (A, a)(1 - x)^{1/4}. \quad (3.1)$$

The constants A, a depend on the dimensionless parameters through the algebraic conditions given in (A 1) and (A 2) in Appendix A.

3.2. Linear perturbation equations

We investigate the linear stability of the steady basic state of §3.1 by introducing small disturbances $h_p, H_p \ll 1$. These give rise to the following linearised perturbation fluxes

$$\mathbf{q}_{lp} = - \left[\frac{\mathcal{M}}{3} h_s^3 (\mathcal{D}\nabla h_p + \nabla H_p) + \frac{\mathcal{M}}{2} h_s^2 (H_s - h_s) \nabla H_p + \mathcal{M} h_s^2 h_p (\mathcal{D}\nabla h_s + \nabla H_s) + \frac{\mathcal{M}}{2} (h_s^2 (H_p - h_p) + 2h_s h_p (H_s - h_s)) \nabla H_s \right], \quad (3.2)$$

$$\begin{aligned}
\mathbf{q}_p = - \left[\frac{1}{3}(H_s - h_s)^3 \nabla H_p + \frac{\mathcal{M}}{2} h_s^2 (H_s - h_s) (\mathcal{D} \nabla h_p + \nabla H_p) \right. \\
+ \mathcal{M} h_s (H_s - h_s)^2 \nabla H_p + (H_s - h_s)^2 (H_p - h_p) \nabla H_s \\
\left. \frac{\mathcal{M}}{2} (2h_s h_p (H_s - h_s) + h_s^2 (H_p - h_p)) (\mathcal{D} \nabla h_s + \nabla H_s) + \right. \\
\left. + \mathcal{M} (h_p (H_s - h_s)^2 + 2h_s (H_s - h_s) (H_p - h_p)) \nabla H_s \right], \tag{3.3}
\end{aligned}$$

and mass conservation equations

$$\frac{\partial h_p}{\partial t} = -\nabla \cdot \mathbf{q}_p, \quad \frac{\partial (H_p - h_p)}{\partial t} = -\nabla \cdot \mathbf{q}_p, \tag{3.4a, b}$$

for the perturbed lower and upper layers, respectively. We impose the boundary conditions

$$\mathbf{q}_p \cdot \mathbf{e}_x = 0, \quad \mathbf{q}_p \cdot \mathbf{e}_x = 0 \quad (x = 0), \tag{3.5a, b}$$

$$h_p = 0, \quad H_p = 0 \quad (x = 1). \tag{3.6a, b}$$

That is, it is required that the source fluxes of both fluids remain fixed and that both fluids drain at the nose.

We search for normal-mode solutions proportional to $e^{\sigma t + iky}$ with amplitudes $\tilde{h}_p(x)$, $\tilde{H}_p(x)$. Here, k is the transverse wave number of the disturbances and σ is their (complex) growth rate. After lengthy algebra, introducing the notation $\xi = 1 - x$ and dropping tildes, the mass conservation equations (3.4a,b) can be written compactly in matrix form

$$\sigma \mathbf{C} \mathbf{v} = \left(\xi^{3/4} \mathbf{E} \mathbf{v}' - \frac{1}{4} \xi^{-1/4} \mathbf{F} \mathbf{v} \right)' - k^2 \xi^{3/4} \mathbf{E} \mathbf{v}, \tag{3.7}$$

and the boundary conditions reduce to

$$\xi^{3/4} \mathbf{E} \mathbf{v}' - \frac{1}{4} \xi^{-1/4} \mathbf{F} \mathbf{v} = 0 \quad (x = 0), \quad \mathbf{v} = 0 \quad (x = 1), \tag{3.8a, b}$$

where the prime denotes differentiation with respect to x . Here, $\mathbf{v} = [h_p, H_p]^T$, and the entries of the matrices \mathbf{C} , \mathbf{E} and \mathbf{F} are given in (A 3)–(A 5) in Appendix A. It will be convenient to define $\mathbf{J} = \mathbf{F} + \mathbf{E}$ and to consider the transformation

$$\tilde{\mathbf{C}} = \mathbf{C} \mathbf{T}, \quad \tilde{\mathbf{E}} = \mathbf{E} \mathbf{T}, \quad \tilde{\mathbf{J}} = \mathbf{J} \mathbf{T}, \tag{3.9a, b, c}$$

where

$$\mathbf{T} = \begin{pmatrix} 1 & 0 \\ 1 & 1 \end{pmatrix}. \tag{3.10}$$

This transformation is equivalent to reformulating the problem in terms of layer thicknesses $[h, H - h]^T$ rather than layer heights $[h, H]^T$. Some key properties of these matrices will prove useful in the later sections, including that the trace and determinant of the $\tilde{\mathbf{E}}$ and $\tilde{\mathbf{J}}$ are strictly positive and that $\tilde{\mathbf{C}}$ is the identity matrix.

We note that (3.7) has a singular point at the front $x = 1$ ($\xi = 0$), which poses a hindrance in our stability calculations. In order to make progress, we analyze the behaviour of the perturbations near this singular point asymptotically in §3.3.

3.3. Asymptotic solution near the singular front

We explore the asymptotic behaviour of the perturbations in an inner region of size $\epsilon \ll 1$ about $\xi = 0$ and define an inner variable $\zeta = \xi/\epsilon$. In terms of this inner variable,

(3.7) becomes

$$\sigma\epsilon^{5/4}\mathbf{C}\mathbf{v} + k^2\epsilon^2\zeta^{3/4}\mathbf{E}\mathbf{v} = \frac{d}{d\zeta} \left(\zeta^{3/4}\mathbf{E}\frac{d\mathbf{v}}{d\zeta} + \frac{1}{4}\zeta^{-1/4}\mathbf{F}\mathbf{v} \right), \quad (3.11)$$

Expanding the solution as a series $\mathbf{v} = \mathbf{v}_0 + \epsilon\mathbf{v}_1 + \dots$ gives, at leading order in ϵ ,

$$\frac{d}{d\zeta} \left(\zeta^{3/4}\mathbf{E}\frac{d\mathbf{v}_0}{d\zeta} + \frac{1}{4}\zeta^{-1/4}\mathbf{F}\mathbf{v}_0 \right) = 0, \quad (3.12)$$

which has general solution

$$\mathbf{v}_0 = \zeta^{1/4}\mathbf{A}_0 + \zeta^{-M}\mathbf{B}_0, \quad (3.13)$$

obtained after direct integration and the use of an integrating factor, where $M = \frac{1}{4}\mathbf{E}^{-1}\mathbf{F}$ and $\mathbf{A}_0, \mathbf{B}_0 \in \mathbb{R}^2$ are constant vectors. The matrix $\zeta^{-M} = \exp(-\log(\zeta)\mathbf{M})$ is defined in terms of its Taylor series. It is possible to show (see (B 3)–(B 4) in Appendix B), that \mathbf{M} is positive definite for all parameter values. This implies that, for nonzero choices of \mathbf{B}_0 , the second term on the right hand side of (3.13) tends to infinity as $\zeta \rightarrow 0$, contradicting the zero-thickness boundary condition (3.8b). This can be seen by changing basis to canonical form. Therefore, $\mathbf{B}_0 = \mathbf{0}$, and so the leading-order solution is simply proportional to $\xi^{1/4}$.

3.4. Stability results

In this section, we show that the system is stable to all perturbations, whatever the choice of the three dimensionless parameters, $\mathcal{M}, \mathcal{D}, \mathcal{Q}$.

After defining $\mathbf{w} = \xi^{-1/4}\mathbf{v}$, equation (3.7) becomes

$$\sigma\xi^{1/4}\mathbf{C}\mathbf{w} + k^2\xi\mathbf{E}\mathbf{w} = \left(\xi\mathbf{E}\mathbf{w}' - \frac{1}{4}\mathbf{J}\mathbf{w} \right)' \quad (3.14)$$

Multiplying on the left by $\mathbf{w}^\dagger\mathbf{J}^\dagger$ and integrating gives

$$\begin{aligned} \sigma \int_0^1 \xi^{1/4}\mathbf{w}^\dagger\mathbf{J}^\dagger\mathbf{C}\mathbf{w}dx + k^2 \int_0^1 \xi\mathbf{w}^\dagger\mathbf{J}^\dagger\mathbf{E}\mathbf{w}dx &= \\ \int_0^1 \mathbf{w}^\dagger\mathbf{J}^\dagger \left(\xi\mathbf{E}\mathbf{w}' - \frac{1}{4}\mathbf{J}\mathbf{w} \right)' dx. & \end{aligned} \quad (3.15)$$

After integrating by parts and noting that $\mathbf{J}^\dagger\mathbf{J}$ is symmetric, the right-hand side becomes

$$\mathbf{w}^\dagger\mathbf{J}^\dagger \left(\xi\mathbf{E}\mathbf{w} - \frac{1}{4}\mathbf{J}\mathbf{w} \right) \Big|_0^1 - \int_0^1 \mathbf{w}^{\dagger\prime}\mathbf{J}^\dagger\mathbf{E}\mathbf{w}'\xi dx + \frac{1}{8}\mathbf{w}^\dagger\mathbf{J}^\dagger\mathbf{J}\mathbf{w} \Big|_0^1. \quad (3.16)$$

Noting that $\xi\mathbf{E}\mathbf{w} - \frac{1}{4}\mathbf{J}\mathbf{w}$ is proportional to $(\mathbf{q}_{lp} \cdot \mathbf{e}_x, \mathbf{q}_p \cdot \mathbf{e}_x)^T$, using the boundary conditions and noting from §3.3 that \mathbf{w} is regular at the nose $x = 1$, we find that

$$\begin{aligned} \sigma \int_0^1 \xi^{1/4}\mathbf{w}^\dagger\mathbf{J}^\dagger\mathbf{C}\mathbf{w}dx + k^2 \int_0^1 \xi\mathbf{w}^\dagger\mathbf{J}^\dagger\mathbf{E}\mathbf{w}dx + \int_0^1 \mathbf{w}^{\dagger\prime}\mathbf{J}^\dagger\mathbf{E}\mathbf{w}'\xi dx &= \\ = -\frac{1}{8}\mathbf{w}^\dagger\mathbf{J}^\dagger\mathbf{J}\mathbf{w} \Big|_{x=1} - \frac{1}{8}\mathbf{w}^\dagger\mathbf{J}^\dagger\mathbf{J}\mathbf{w} \Big|_{x=0} &\leq 0. \end{aligned} \quad (3.17)$$

We wish to show that $\mathbf{J}^\dagger\mathbf{C}$ and $\mathbf{J}^\dagger\mathbf{E}$ are both positive definite as this implies that each of the integrals on the left hand side of (3.17) are strictly positive for nonzero perturbations \mathbf{w} . This implies that $\sigma \leq 0$, else, if $\sigma > 0$ then the left hand side of (3.17) is strictly positive while the right hand side is negative – a contradiction. It is sufficient to show that $\tilde{\mathbf{J}}^\dagger\tilde{\mathbf{C}}$ and $\tilde{\mathbf{J}}^\dagger\tilde{\mathbf{E}}$ are positive definite. After some algebra and using the fact that $A > 0$ and $A > a$, it is possible to show that $\tilde{\mathbf{E}}$ and $\tilde{\mathbf{J}}$ have all strictly positive entries,

hence the trace of both matrices is strictly positive, and that their determinants are also strictly positive. Therefore, $\tilde{\mathbf{E}}$ and $\tilde{\mathbf{J}}$ are positive definite. Since $\tilde{\mathbf{E}}$ and $\tilde{\mathbf{J}}$ have strictly positive entries, so does the product $\tilde{\mathbf{J}}^\dagger \tilde{\mathbf{E}}$, and in particular, the trace of this product is strictly positive. Using this and the fact that $\det(\tilde{\mathbf{J}}^\dagger \tilde{\mathbf{E}}) = \det(\tilde{\mathbf{J}}) \det(\tilde{\mathbf{E}}) > 0$, we conclude that $\tilde{\mathbf{J}}^\dagger \tilde{\mathbf{E}}$, and hence $\mathbf{J}^\dagger \mathbf{E}$, is positive definite. See Appendix C for details, in particular (C5), (C10) and the surrounding text. Note also that $\tilde{\mathbf{C}} \equiv \mathbf{I}$ is the identity matrix, therefore, $\tilde{\mathbf{J}}^\dagger \tilde{\mathbf{C}} = \tilde{\mathbf{J}}^\dagger$, and hence $\mathbf{J}^\dagger \mathbf{C}$, is positive definite as well. This concludes the argument that $\sigma \leq 0$. This conclusion holds for all values of the dimensionless parameters $\mathcal{M}, \mathcal{D}, \mathcal{Q}$. That is, it is not possible to find a choice of parameters for which the system is linearly unstable to small perturbations.

3.5. One-layer gravity currents with drainage

Although the framework above was developed for lubricated, two-layer currents, it may also be applied to a single-fluid current by taking $\mathcal{Q} = 0$. The shape of the steady state current remains qualitatively the same, except that $a = 0$ and, by (A2), $A = 12^{1/4}$. There are no free dimensionless parameters in this case. Although the matrices used in the previous sections are no longer well defined, we can instead straightforwardly show that the perturbation H_p obeys the perturbation equation (3.7) with \mathbf{C} replaced by the scalar $3/A^3$, \mathbf{E} replaced by 1, and \mathbf{F} by 3. As these are all strictly positive scalars, by following the analysis of §3.4 it is immediate that the one-layer gravity current with drainage is linearly stable as well, as expected.

4. Frontal dynamics: mechanism of instability at the lubrication front

The results of the previous section suggest that the experimentally observed fingering originates from a frontal, rather than internal, instability. This is consistent with a previous study on two-layer flow down an incline, where it was illustrated that modes with no transverse variation are stable (Toniolo 2001).

The basic state for the problem we wish to investigate is non-standard in that it is both time- and space-dependent, and normal-mode solutions do not, in general, exist. We proceed by splitting the domain of the flow into two asymptotic regions in a two-dimensional geometry: an active, inner region near the lubrication front, in which the onset of instability occurs, and a passive, outer region away from the lubrication front, in which the perturbations decay as the lubrication front is distanced. The inner and outer regions are matched asymptotically through decay conditions.

By also assuming that the changes in surface heights near the lubrication front are small and that the growth rate of the perturbations is much faster than that of the basic state (a frozen-time approximation), this reduces the perturbation equations to a system of linear differential equations with normal-mode solutions that have space-dependent amplitudes in the inner region. Both of these assumptions are encapsulated in a single rescaling.

In this section, we confine attention to the region near the lubrication front, illustrated in figure 2b, and consider the limit in which the flow of both the basic state and the perturbations is resisted dominantly by vertical shear stresses. We begin by discussing the mechanism of instability and follow on with a formal derivation of the instability threshold.

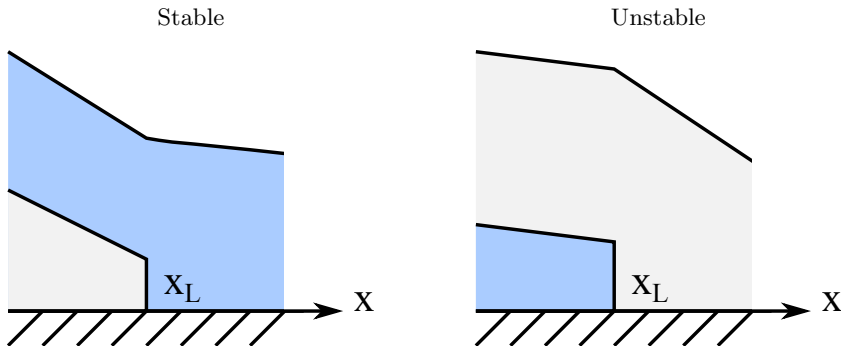


Figure 3: Schematic of stable and unstable flow configurations. Here, $\mathcal{M} < 1$ (the lower layer is more viscous) in the left-hand panel, whereas $\mathcal{M} > 1$ (the lower layer is less viscous) in the right-hand panel.

4.1. Mechanism of instability

To illustrate the instability mechanism, consider the case $\mathcal{M} > 1$ in which a less viscous fluid intrudes into a more viscous fluid in the unlubricated region, depicted in the right-hand panel of Figure 3. In this case, surface slopes, and so pressure gradients, are larger in the unlubricated region than in the lubricated region. If the front is perturbed and the less viscous fluid finds itself in the unlubricated region, it will become subject to higher hydrostatic pressure gradients and so will advance forward, causing an instability. The scenario is reversed in the opposite case $\mathcal{M} < 1$, depicted in the left-hand panel of Figure 3. In this case, the jump in slope is reversed so that surface slopes, and so pressure gradients, are smaller in the unlubricated region than in the lubricated region and if the front is perturbed so that the more viscous, underlying fluid gets displaced past the position of the basic state front, then it will become subject to lower hydrostatic pressure gradients and become suppressed. That is, a viscosity contrast brings with it a change in pressure gradient, which triggers the instability.

There is a fundamental similarity between this instability and the Saffman-Taylor instability in that both are caused by discontinuities in a driving pressure gradient. However, in this case, the underlying pressure gradients originate from changes in free-surface slope and are related to hydrostatic pressure rather than dynamic pressure.

We proceed with a formal justification of the physical mechanism in the following sections.

4.2. Perturbations resisted by vertical shear

We use the non-dimensionalisation (2.2), for which we use the lengthscale

$$\mathcal{L} = \left(\frac{gq_0^3 T_0^4}{\nu} \right)^{1/5}, \quad (4.1)$$

where T_0 is the time delay between the initiation of flow of the two layers, as in the experiments of Kowal & Worster (2015). The shear-dominated theory of §2 is supplemented by the following mass conservation equations in the no-slip region

$$\mathbf{q} = -\frac{1}{3}H^3\nabla H, \quad \frac{\partial H}{\partial t} = -\nabla \cdot \mathbf{q} \quad (x \geq x_L), \quad (4.2)$$

(Huppert 1982), the matching condition

$$[H]_-^+ = 0 \quad (x = x_L), \quad (4.3a, b)$$

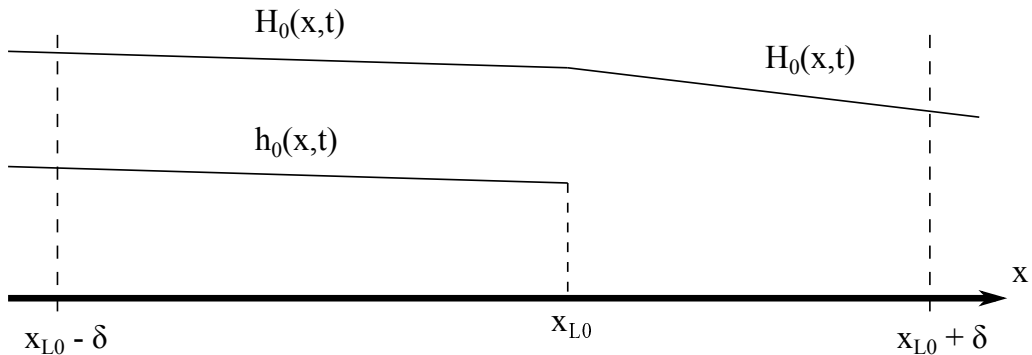


Figure 4: Schematic of the basic state in the inner region, in which the surface heights are locally linear.

at the lubrication front, and the flux condition and kinematic condition

$$\left[\mathbf{q} \cdot \mathbf{n}_L + \mathbf{q}_l \cdot \mathbf{n}_L \right]^- = \left[\mathbf{q} \cdot \mathbf{n}_L \right]^+ \quad (x = x_L), \quad (4.4)$$

$$\mathbf{n}_L \cdot \dot{\mathbf{x}}_L = \lim_{x \rightarrow x_L} \mathbf{n}_L \cdot \mathbf{q}_l / h. \quad (4.5)$$

Here, we take $\mathcal{D} = 0$.

4.3. Linearisation

We investigate the linear stability of the system by introducing small disturbances of size $\epsilon \ll 1$ (distinct from ϵ used in the previous section) and write $h = h_0 + \epsilon h_1$, $H = H_0 + \epsilon H_1$, $x_L = x_{L0} + \epsilon x_{L1}$ and so on. These give rise to the following linearised perturbation fluxes

$$\mathbf{q}_{11} = - \left[\left(-\frac{\mathcal{M}}{2} h_0^2 h_1 + \mathcal{M} h_0 h_1 H_0 + \frac{\mathcal{M}}{2} h_0^2 H_1 \right) \nabla H_0 + \left(-\frac{\mathcal{M}}{6} h_0^3 + \frac{\mathcal{M}}{2} h_0^2 H_0 \right) \nabla H_1 \right], \quad (4.6)$$

$$\mathbf{q}_1 + \mathbf{q}_{11} = - \left[((1 - \mathcal{M})(H_0 - h_0)^2 (H_1 - h_1) + \mathcal{M} H_0^2 H_1) \nabla H_0 + \left(\frac{1 - \mathcal{M}}{3} (H_0 - h_0)^3 + \frac{\mathcal{M}}{3} H_0^3 \right) \nabla H_1 \right], \quad (4.7)$$

in the lubricated region and

$$\mathbf{q}_1 = - \left[H_0^2 H_1 \nabla H_0 + \frac{1}{3} H_0^3 \nabla H_1 \right], \quad (4.8)$$

in the unlubricated region. First-order mass-conservation equations in the lubricated region are

$$\frac{\partial h_1}{\partial t} = -\nabla \cdot \mathbf{q}_{11}, \quad \frac{\partial (H_1 - h_1)}{\partial t} = -\nabla \cdot \mathbf{q}_1, \quad (4.9a, b)$$

and in the unlubricated region

$$\frac{\partial H_1}{\partial t} = -\nabla \cdot \mathbf{q}_1. \quad (4.10)$$

The condition of flux continuity to first order in ϵ can be expressed as

$$\left[x_{L1} \frac{\partial}{\partial x} (\mathbf{q}_{10} + \mathbf{q}_0) + (\mathbf{q}_{11} + \mathbf{q}_1) \right]^- \cdot \mathbf{e}_x = \left[x_{L1} \frac{\partial}{\partial x} \mathbf{q}_0 + \mathbf{q}_1 \right]^+ \cdot \mathbf{e}_x \quad (x = x_{L0}). \quad (4.11)$$

Height continuity to first order gives

$$\left[x_{L1} \frac{\partial H_0}{\partial x} + H_1 \right]^- = \left[x_{L1} \frac{\partial H_0}{\partial x} + H_1 \right]^+ \quad (x = x_{L0}), \quad (4.12)$$

and the kinematic condition to first order gives

$$\dot{x}_{L1} = \frac{1}{h_0} \left(x_{L1} \frac{\partial \mathbf{q}_{10}}{\partial x} + \mathbf{q}_{11} \right) \cdot \mathbf{e}_x - \frac{\mathbf{q}_{10} \cdot \mathbf{e}_x}{h_0^2} \left(x_{L1} \frac{\partial h_0}{\partial x} + h_1 \right). \quad (4.13)$$

We wish to perform a local analysis in an inner region of size $\delta \ll x_L$ near the lubrication front in which the surface heights of the two layers in the lubricated region as well as that of the unlubricated region are linear to first order in δ . This can be attained by rescaling

$$x - x_{L0} = \delta(\tilde{x} - x_{L0}), \quad y = \delta\tilde{y}, \quad t - 1 = \delta^2\tilde{t}, \quad (4.14)$$

assuming $\tilde{x}, \tilde{y}, \tilde{t} = \mathcal{O}(1)$ as $\delta \rightarrow 0$, and expanding to first order in δ . Such an approach can be justified by identifying δ with k^{-1} . Such an approach also ensures that the linearised quantities are independent of time, which, effectively, imposes a frozen-time approximation. We additionally impose that all perturbations are local to the lubrication front and decay away from it. We present a more detailed analysis, involving the full region of the flow and perturbation equations involving the full, space-dependent basic state in the companion paper (Kowal & Worster 2018).

In what follows, we split the domain of the flow into two asymptotic regions: the above-mentioned inner region near the lubrication front, composed of both the lubricated and no-slip domains, and two outer regions away from the lubrication front, which also consist of both the lubricated and no-slip domains.

Evaluating basic state quantities at $t = 1$ defines the dimensional time scale \mathcal{T} . We denote the basic-state surface heights in the inner region to first order in δ by

$$h_0 = a + b(x - x_L), \quad H_0 = A + B(x - x_L) \quad (x \leq x_{L0}) \quad (4.15a, b)$$

for the lubricated region, and

$$H_0 = \alpha + \beta(x - x_L) \quad (x \geq x_{L0}) \quad (4.16)$$

for the unlubricated region, as depicted in the schematic diagram of Figure 4.

By searching for normal-mode solutions in the frame of the lubrication front and writing

$$(h_1(x, y, t), H_1(x, y, t), x_{L1}(y, t)) = (\hat{h}_1(x), \hat{H}_1(x), \hat{x}_{L1}) \exp(\sigma t +iky), \quad (4.17)$$

where k is the transverse wave number of the disturbances and σ is their (complex) growth rate, we find that the amplitudes satisfy the following mass conservation equations (after dropping hats)

$$\sigma h_1 - V h_1' = \left(a_{11} H_0' + a_{12} H_1' \right)' - a_{13} k^2 H_1 \quad (x \leq x_{L0}), \quad (4.18)$$

$$\sigma H_1 - V H_1' = \left(a_1 H_0' + a_2 H_1' \right)' - a_3 k^2 H_1 \quad (x \leq x_{L0}), \quad (4.19)$$

for the lubricated region and

$$\sigma H_1 - V H_1' = \left[H_0^2 H_1 H_0' + \frac{1}{3} H_0^3 H_1' \right]' - \frac{k^2}{3} H_0^3 H_1 \quad (x \geq x_{L0}), \quad (4.20)$$

for the unlubricated region, where a_i, a_i , for $i = 1, \dots, 3$, are cubic functions of the basic state layer thicknesses and the viscosity ratio \mathcal{M} , which are given in (S.1)–(S.9) of the Supplementary Material. Here, $V = \dot{x}_{L0}$ is the velocity of the lubrication front, which is related to A, B, a, b through its dependence on the three dimensionless parameters. Of interest to us are the equations (4.18)–(4.20) up to first order in δ (see (D 1)–(D 3) of Appendix D for details).

The first-order flux continuity boundary condition reduces to

$$\left\{ \bar{c}_1 x_{L1} + \bar{c}_2 H_1 + \bar{c}_3 h_1 + \bar{c}_4 \frac{\partial H_1}{\partial x} \right\}^- = \left\{ x_{L1} \alpha^2 \beta^2 + \alpha^2 \beta H_1 + \frac{1}{3} \alpha^3 \frac{\partial H_1}{\partial x} \right\}^+, \quad (4.21)$$

for $x = x_{L0}$, where $\bar{c}_1, \dots, \bar{c}_4$ are functions of the viscosity ratio \mathcal{M} , the basic state thicknesses a, A , and slopes b, B , and are given in (S.43)–(S.46) of the Supplementary Material. Similarly, the condition for continuity of height becomes

$$\left[x_{L1} B + H_1 \right]^- = \left[x_{L1} \beta + H_1 \right]^+ \quad (4.22)$$

for $x = x_{L0}$. The kinematic condition becomes

$$\sigma x_{L1} = \mathcal{M} \left(c_8 x_{L1} + c_9 h_1 + c_{10} H_1 + c_{11} \frac{\partial H_1}{\partial x} \right) \quad (4.23)$$

for $x = x_{L0}^-$, where c_8, \dots, c_{11} are functions of the layer thicknesses and their derivatives, and are given in (S.47)–(S.50) of the Supplementary Material.

The equations (4.18)–(4.20) up to first order in δ along with the boundary conditions (4.21)–(4.23) form a system of linear differential equations with constant coefficients, with solutions of the form

$$\begin{aligned} (h_1, H_1) &= (\tilde{h}_1^-, \tilde{H}_1^-) \exp((x - x_{L0})\lambda^-) \quad (x \leq x_{L0}), \\ H_1 &= \tilde{H}_1^+ \exp((x - x_{L0})\lambda^+) \quad (x \geq x_{L0}) \end{aligned} \quad (4.24a, b)$$

where $\tilde{h}_1^-, \tilde{H}_1^-, \tilde{H}_1^+$ are constants. Direct substitution into the mass conservation equations (D 1)–(D 3) and corresponding matching conditions yields a system of six algebraic equations for the six unknown variables $\sigma, x_{L1}, \tilde{h}_1^-, \tilde{H}_1^+, \lambda^-, \lambda^+$, where it has been assumed that $\tilde{H}_1^- \equiv 1$, without loss of generality, as solutions of this eigenproblem are defined only up to a multiplicative constant. We restrict the choice of solutions to those that decay exponentially from the lubrication front, giving that $\lambda^- > 0$ and $\lambda^+ < 0$.

Expressing the mass conservation equations in the lubricated region in matrix form gives

$$(\mathbf{P} - (\sigma - V\lambda^-)\mathbf{I})[\tilde{h}_1^-, \tilde{H}_1^-]^T = \mathbf{0} \quad (4.25)$$

where \mathbf{P} is a 2×2 matrix with entries that are a function of λ^-, k, a, A, b, B , and \mathcal{M} . The entries of \mathbf{P} are given explicitly in (S.51)–(S.54) of the Supplementary Material. Requiring non-trivial solutions gives that λ^- satisfies

$$\det(\mathbf{P} - (\sigma - V\lambda^-)\mathbf{I}) = 0, \quad (4.26)$$

which is a cubic equation for λ^- . Recalling that $\tilde{H}_1^- = 1$, without loss of generality, it

follows that \tilde{h}_1^- is given by the corresponding solution to (4.26), that is,

$$\tilde{h}_1^- = \frac{(a(b(6B - 3a\lambda^- + 6A\lambda^-) + a(6B\lambda^- + (a - 3A)(k - \lambda^-)(k + \lambda^-)))\mathcal{M})}{(3B(-2Ab + a^2\lambda^- + 2a(b - B - A\lambda^-))\mathcal{M} + 6\sigma - 6V\lambda^-)} \quad (4.27)$$

Solving the mass conservation equation within the unlubricated region subject to decay conditions gives λ^+ explicitly as

$$\lambda^+ = -\frac{1}{2\alpha^3}(6\alpha^2\beta + 3V + \sqrt{4\alpha^3(3\alpha\beta^2 + \alpha^3k^2 + 3\sigma) + 36\alpha^2\beta V + 9V^2}) \quad (4.28)$$

The flux continuity condition specifies the dispersion relation for σ in the form

$$\zeta_1 x_{L1} + \zeta_2 \tilde{H}_1^- + \zeta_3 \tilde{h}_1^- = -\frac{1}{3}\alpha^2(3\beta\tilde{H}_1^+ + \alpha\tilde{H}_1^+\lambda^+ + 3\beta^2 x_{L1}), \quad (4.29)$$

where ζ_1, \dots, ζ_3 are functions of a, A, b, B, \mathcal{M} and λ^- and are given in (S.55)–(S.57) of the Supplementary Material. This is an implicit equation for σ , which appears via λ^- and λ^+ . The λ^- and λ^+ appear linearly in the dispersion relation and are solutions of cubic and quadratic equations, respectively. More than one solution for λ^- and λ^+ , and hence, for σ are possible and we are interested in the solution for which the real part of σ is largest. \tilde{H}_1^+ and x_{L1} are found by using the height continuity and kinematic conditions to be

$$\tilde{H}_1^+ = x_{L1}(B - \beta) + \tilde{H}_1^-, \quad (4.30)$$

and

$$x_{L1} = \frac{1}{\zeta_6}(\zeta_4 \tilde{h}_1^- + \zeta_5 \tilde{H}_1^-) \quad (4.31)$$

where ζ_4, \dots, ζ_6 are functions of $a, A, b, B, \mathcal{M}, \sigma$ and λ^- and are given in (S.58)–(S.60) of the Supplementary Material.

In this section, we have determined the dispersion relation for σ in terms of quantities such as the perturbations to the surface heights and leading edge position. Equations in this section are solved numerically and the solutions for σ are shown in figure 5. In order to formulate a stability criterion, we wish to simplify these using large-wavenumber asymptotics in the following section.

4.4. Large- k asymptotics

In what follows, we expand in series of $1/k$ for k large and write $X = X_0k + X_1 + \dots$, where $X = (\sigma, \lambda^\pm, \tilde{H}_1^\pm, \tilde{h}_1^-, x_{L1})$. Using (4.26) gives the leading-order governing equation in the lubricated region

$$\frac{1}{6}k^3[(\lambda_0^-)^2 - 1][\lambda_0^- - \tilde{\lambda}_0^-] = \mathcal{O}(k^2) \quad (4.32)$$

giving $\lambda_0^- = \pm 1$ or $\lambda_0^- = \tilde{\lambda}_0^-$ where

$$\tilde{\lambda}_0^- = -\frac{2\sigma_0 \tilde{\lambda}_{n0}}{\tilde{\lambda}_{d0}} \quad (4.33)$$

and $\tilde{\lambda}_{n0}, \tilde{\lambda}_{d0}$ are functions of the layer thicknesses, slopes, the viscosity ratio \mathcal{M} and V . Explicit expressions are given in (S.61)–(S.62) of the Supplementary Material. It can be deduced from the latter expression that $\tilde{\lambda}_0^- \rightarrow 0$ as $\mathcal{M} \rightarrow 0$. Taking $\lambda_0^- = 1$ gives the next order equation outlined in the Supplementary Material, which gives the next order

contribution

$$\lambda_1^- = \frac{\lambda_{n1}^-}{\lambda_{d1}^-}, \quad (4.34)$$

where λ_{n1}^- , λ_{d1}^- are given in (S.64)–(S.65) of the Supplementary Material. The relation (4.27) between \tilde{h}_1^- and \tilde{H}_1^- , given without loss of generality that $\tilde{H}_0^- = 1$, yields

$$\tilde{h}_{10}^- k + \tilde{h}_{11}^- + \mathcal{O}(1/k) = \frac{\zeta_7}{\zeta_8}, \quad (4.35)$$

where ζ_7 , ζ_8 are given in (S.66)–(S.67) of the Supplementary Material. ζ_7 , ζ_8 are functions of k , among other quantities. Expanding in series of $1/k$ gives that $\tilde{h}_{10}^- = 0$ and

$$\tilde{h}_{11}^- = \left[\frac{a\mathcal{M}(6Ab - 2a^2\lambda_1^- + a(-3b + 6(B + A\lambda_1^-)))}{3a(a - 2A)B\mathcal{M} + 6(\sigma_0 - V)} \right]. \quad (4.36)$$

The governing equation (4.28) for the unlubricated region gives that

$$\begin{aligned} \lambda_0^+ k + \lambda_1^+ \mathcal{O}(1/k) &= \frac{1}{2} \left[-\frac{6\beta}{\alpha} - \frac{3V}{\alpha^3} - \sqrt{4\alpha^6 k^2 + 12\alpha^3 \sigma_0 k + \mathcal{O}(1)} \right] \\ &= -k - \frac{3}{2} \left[2\frac{\beta}{\alpha} + \frac{\sigma_0 + V\lambda^+}{\alpha^3} \right] + \mathcal{O}(1/k), \end{aligned} \quad (4.37)$$

and so $\lambda_0^+ = -1$ and $\lambda_1^+ = -\frac{3}{2} \left[2\frac{\beta}{\alpha} + \frac{\sigma_0 + V\lambda^+}{\alpha^3} \right]$. The kinematic condition gives that

$$x_{L10} = 0, \quad (4.38)$$

$$x_{L11} = -\frac{2(A - a)^3 + 3a(2A - a)(A - a)\mathcal{M}}{6a\sigma_0}, \quad (4.39)$$

$$(4.40)$$

The next-order contribution, x_{L12} , which will be needed in determining the first-order correction to the dispersion relation (note x_{L11} was needed in determining the dispersion relation at leading order), is given in (S.68) of the Supplementary Material. The height continuity condition gives

$$\begin{aligned} \tilde{H}^+ &= x_{L1}(B - \beta) + \tilde{H}^- \\ &= x_{L11}(B - \beta) + \tilde{H}_{11}^- + x_{L12}(B - \beta)\frac{1}{k} + \mathcal{O}(1/k^2) \end{aligned} \quad (4.41)$$

and so

$$\tilde{H}_{10}^+ = 0, \quad \tilde{H}_{11}^+ = x_{L11}(B - \beta) + \tilde{H}_{11}^-, \quad \tilde{H}_{12}^+ = x_{L12}(B - \beta). \quad (4.42a - c)$$

The leading-order flux condition reduces to

$$\tilde{H}_{11}^+ = \left[(1 - \mathcal{M})(1 - a/A)^3 + \mathcal{M} \right] \frac{\tilde{H}_{11}^-}{\lambda_0^+}, \quad (4.43)$$

which, by comparison to (4.42b), gives

$$\sigma_0 = \gamma(a, A, \mathcal{M})(B - \beta) \quad (4.44)$$

where

$$\gamma(a, A, \mathcal{M}) = \frac{A - a}{6a} \cdot \frac{2(A - a)^2 + 3a(2A - a)\mathcal{M}}{(\mathcal{M} + 1) + (1 - a/A)^3(1 - \mathcal{M})}. \quad (4.45)$$

4.5. *Instability threshold*

The formula (4.44) shows that to leading order, the growth rate behaves as

$$\sigma \sim -k\gamma(a, A, \mathcal{M}) \left[\frac{\partial H_0}{\partial x} \right]_{-}^{+}, \quad (4.46)$$

at $x = x_{L0}$, as $k \rightarrow \infty$. That is, the growth rate varies linearly with k , as $k \rightarrow \infty$, which signifies that there is no stabilising mechanism at large wavenumbers under the physics considered so far, similarly to the original result of Saffman & Taylor (1958) for the onset of viscous fingering in a porous medium without the stabilising influence of surface tension. We explore possible stabilising mechanisms in §5 and 6 of this paper and in the companion paper. Since $\gamma(a, A, \mathcal{M})$ in this expression is a positive constant, one can deduce that there are positive growth rates at large wave numbers precisely when

$$\frac{\partial H_0}{\partial x}^{-} > \frac{\partial H_0}{\partial x}^{+} \quad (x = x_{L0}), \quad (4.47)$$

that is, when the upper surface slope is gentler in the lubricated region than in the unlubricated region: $|\partial H_0^{-}/\partial x| < |\partial H_0^{+}/\partial x|$, since the surface slopes are negative.

To understand the conditions under which precisely this break in slope occurs, the condition of continuity of flux for the basic state $(\mathbf{q}_0 + \mathbf{q}_{10})^{-} \cdot \mathbf{e}_x = \mathbf{q}_0^{+} \cdot \mathbf{e}_x$, written explicitly as,

$$\left\{ -\frac{1}{3} \left[(1 - \mathcal{M})(H_0 - h_0)^3 + \mathcal{M}H_0^3 \right] \frac{\partial H_0}{\partial x} \right\}^{-} = \left\{ -\frac{1}{3} H_0^3 \frac{\partial H_0}{\partial x} \right\}^{+}, \quad (4.48)$$

may be used to relate the upstream and downstream upper surface slopes as

$$\beta = \left[(1 - \mathcal{M})(1 - a/A)^3 + \mathcal{M} \right] B, \quad (4.49)$$

showing that B and β have the same sign (negative), since the prefactor on the right-hand side is positive, and that the condition $B > \beta$ is equivalent to

$$\left[(1 - \mathcal{M})(1 - a/A)^3 + \mathcal{M} \right] > 1, \quad (4.50)$$

that is,

$$(\mathcal{M} - 1) \left[1 - (1 - a/A)^3 \right] > 0, \quad (4.51)$$

or, equivalently,

$$\mathcal{M} > 1. \quad (4.52)$$

Therefore, the jump in slope is completely determined by the viscosity ratio between the two fluids, which further determines the stability of the front at large wave numbers.

4.6. *Higher-order contributions*

In order to determine an asymptotic solution, such that the difference between it and the full numerical solution decays to zero as $k \rightarrow \infty$, we examine the next order. This provides visual agreement between asymptotic and numerical results for moderate wavenumbers. To the next order, the flux condition gives

$$\tilde{H}_{12}^{+} = \phi_1 \tilde{h}_{11}^{-} + \phi_2 \tilde{H}_{11}^{-} + \phi_3 \tilde{H}_{11}^{+} + \phi_4 x_{L11}, \quad (4.53)$$

where ϕ_1, \dots, ϕ_4 are given in (S.69)–(S.72) of the Supplementary Material. Relating this to (4.42c) gives the next order correction for the growth rate

$$\sigma_1 = \phi_5 \tilde{h}_{11}^{-} + \phi_6 \tilde{H}_{11}^{-} + \phi_7 \tilde{H}_{11}^{+} + \phi_8 x_{L11}, \quad (4.54)$$

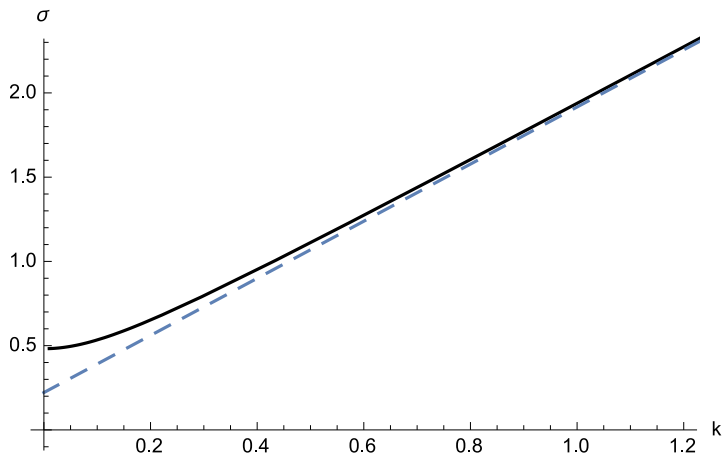


Figure 5: Asymptotic (dashed) and numerical (solid) solutions of the equations of §4 for the growth rates σ against wavenumber k for perturbations resisted dominantly by vertical shear. Parameter values used are $\mathcal{M} = 10$ and $\mathcal{Q} = 0.1$.

where the coefficients ϕ_5, \dots, ϕ_8 are given in (S.73)–(S.76) of the Supplementary Material.

The asymptotic solution

$$\sigma \sim \sigma_0 k + \sigma_1 \quad (k \rightarrow \infty), \quad (4.55)$$

where σ_0 and σ_1 are derived above, is compared against the numerical solution for σ against k in Figure 5. The asymptotic solution is shown to converge towards the numerical solution (solid curve in figure 5) as k increases, with good agreement obtained for $k \gtrsim 0.5$.

It is seen from the asymptotic solution that the growth rates increase unboundedly as the wavenumber increases. Therefore, the limit in which vertical shear provides the dominant resistance to the flow of the perturbations provides no stabilising mechanism for large wavenumbers, indicating that there is another physical mechanism in our experiments that stabilises the flow for large-enough wavenumbers. To explore one such possible mechanism, we consider the effect of horizontal shear as the dominant resistance to the flow of the perturbations in the next section. Horizontal shear stresses become important (or dominate) when the wavelength of the perturbations is comparable to (or much smaller than) the thickness of both layers of fluid. The next section concerns the latter limit.

5. Frontal dynamics: stabilisation by horizontal shear

For large enough wavenumbers, the wavelength of the perturbations is much smaller than the vertical length scale and the perturbations become resisted dominantly by horizontal shear stresses. This occurs in both layers when $k \geq 1/h$. We wish to consider this limit in this section, and explore whether it stabilizes the flow for large wavenumbers.

5.1. Model equations

5.1.1. Unlubricated region

To investigate the stability of the flow, we introduce small disturbances of size $\epsilon \ll 1$ and search for normal-mode solutions with transverse wavenumber k and growth rate σ of the form $X = X_0 + \epsilon X_1 + \dots$, where $X_1 = \hat{X}_1 \exp(iky + \sigma t)$ and $X = (H(x, y, t), \mathbf{u}(x, y, z, t), \mathbf{q}(x, y, t))$. With the assumption that the perturbations to the

flow are resisted dominantly by horizontal shear stresses, the gradients in z are negligible and so the perturbation to the velocity obeys

$$\mathbf{u}_1 = -\frac{1}{k^2} \nabla H_1. \quad (5.1)$$

In contrast with the previous analysis, here the velocity involves a $1/k^2$ contribution, reflecting the resistance to the flow by horizontal shear stresses. We will use the convention that the y -component of the gradient operator means either d/dy or ik , interchangeably.

The volume flux, per unit width, can be expressed as

$$\mathbf{q} = \int_0^H \mathbf{u} dz = \int_0^{H_0 + \epsilon H_1} (\mathbf{u}_0 + \epsilon \mathbf{u}_1) dz \quad (5.2)$$

$$= \int_0^{H_0} \mathbf{u}_0 dz + \epsilon \left[\int_0^{H_0} \mathbf{u}_1 dz + H_1 \mathbf{u}_0 \Big|_{z=H_0} \right] + \mathcal{O}(\epsilon^2) \quad (5.3)$$

so that the perturbation to the volume flux, per unit width, is

$$\mathbf{q}_1 = \int_0^{H_0} \mathbf{u}_1 dz + H_1 \mathbf{u}_0 \Big|_{z=H_0} = \int_0^{H_0} \mathbf{u}_1 dz - \frac{1}{2} H_1 H_0^2 \nabla H_0 \quad (5.4)$$

since the basic state velocity for a classical current is primarily along the x -direction with $u_0 = -\frac{1}{2}z(2H_0 - z)\partial H_0/\partial x$. Substituting the expression (5.1) for the perturbation to the velocity gives

$$\mathbf{q}_1 = -\frac{1}{k^2} H_0 \nabla H_1 - \frac{1}{2} H_1 H_0^2 \nabla H_0 \quad (5.5)$$

This differs from (4.8) in the $1/k^2$ term to reflect that the flow of the perturbations is resisted by horizontal shear. The time-evolution of the perturbations, in the frame of the lubrication front, is governed by the mass conservation equation for the next order in ϵ

$$\begin{aligned} \sigma H_1 - V \frac{\partial H_1}{\partial x} &= -\nabla \cdot \mathbf{q}_1 \\ &= -\frac{\partial}{\partial x} (\mathbf{q}_1 \cdot \mathbf{e}_x) - ik \mathbf{q}_1 \cdot \mathbf{e}_y. \end{aligned} \quad (5.6)$$

5.1.2. Lubricated region

We introduce small perturbations of size $\epsilon \ll 1$ and investigate the stability of the flow by searching for normal-mode solutions with transverse wavenumber k and growth rate σ . We expand in series of ϵ , $Y = Y_0 + \epsilon Y_1$ where $Y_1 = \hat{Y}_1 \exp(iky + \sigma t)$, and

$$Y = [H(x, y, t), h(x, y, t), \mathbf{u}(x, y, z, t), \mathbf{u}_l(x, y, z, t), \mathbf{q}(x, y, t), \mathbf{q}_l(x, y, t)]. \quad (5.7)$$

As the perturbations to the flow are resisted dominantly by horizontal shear stresses, the gradients in z are negligible and so

$$\mathbf{u}_1 = -\frac{1}{k^2} \nabla H_1 \quad (5.8)$$

for the upper layer and

$$\mathbf{u}_{l1} = -\frac{\mathcal{M}}{k^2} \nabla H_1 \quad (5.9)$$

for the lower layer. There is a small boundary layer at the interface between the two fluids and at the base, in which vertical shear stresses are important and resolve the no-slip boundary condition as well as the continuity of velocity and shear stress at the interface. However, the effect of this boundary layer is negligible in a depth-averaged description of

the flow when the wavenumber of the perturbations is large, specifically, when $k \gg 1/h$. As an alternative to scaling arguments, this can also be deduced from considering the full calculation with $k = \mathcal{O}(1)$ so that both vertical and transverse shear contribute to resisting the perturbations to the flow, and considering the limit $kh \rightarrow \infty$.

The volume flux, per unit width, of the upper layer fluid is

$$\begin{aligned} \mathbf{q} &= \int_h^H \mathbf{u} dz = \int_{h_0+\epsilon h_1}^{H_0+\epsilon H_1} (\mathbf{u}_0 + \epsilon \mathbf{u}_1) dz \\ &= \int_{h_0}^{H_0} \mathbf{u}_0 dz + \epsilon \left[\int_{h_0}^{H_0} \mathbf{u}_1 dz + H_1 \mathbf{u}_0 \Big|_{z=H_0} - h_1 \mathbf{u}_0 \Big|_{z=h_0} \right] + \mathcal{O}(\epsilon^2) \end{aligned} \quad (5.10)$$

and in the lower layer,

$$\begin{aligned} \mathbf{q}_l &= \int_0^h \mathbf{u}_l dz = \int_0^{h_0+\epsilon h_1} (\mathbf{u}_{l0} + \epsilon \mathbf{u}_{l1}) dz \\ &= \int_0^{h_0} \mathbf{u}_{l0} dz + \epsilon \left[\int_0^{h_0} \mathbf{u}_{l1} dz + h_1 \mathbf{u}_{l0} \Big|_{z=h_0} \right] + \mathcal{O}(\epsilon^2). \end{aligned} \quad (5.11)$$

By using expressions for the velocity fields for the two layers at zeroth order in ϵ given Kowal & Worster (2015), the perturbation to the volume flux in the upper layer can be found to be

$$\begin{aligned} \mathbf{q}_1 &= -\frac{1}{k^2}(H_0 - h_0)\nabla H_1 - \frac{1}{2}(H_1 - h_1) \left[\mathcal{M}h_0^2 \right. \\ &\quad \left. + 2\mathcal{M}h_0(H_0 - h_0) \right] \nabla H_0 - \frac{1}{2}H_1(H_0 - h_0)^2 \nabla H_0 \end{aligned} \quad (5.12)$$

and in the lower layer,

$$\mathbf{q}_{l1} = -\frac{1}{k^2}\mathcal{M}H_0\nabla H_1 - \frac{1}{2}h_1 \left[\mathcal{M}h_0^2 + 2\mathcal{M}h_0(H_0 - h_0) \right] \nabla H_0. \quad (5.13)$$

These differ from (4.6) and (4.7) in the $1/k^2$ term, as before. Conservation of mass at first order in ϵ in the two layers is described by

$$\begin{aligned} \sigma(H_1 - h_1) - V(H'_1 - h'_1) &= -\nabla \cdot \mathbf{q}_1 \\ &= -\frac{\partial}{\partial x}(\mathbf{q}_1 \cdot \mathbf{e}_x) - ik\mathbf{q}_1 \cdot \mathbf{e}_y \end{aligned} \quad (5.14)$$

for the upper layer and

$$\begin{aligned} \sigma h_1 - V h'_1 &= -\nabla \cdot \mathbf{q}_{l1} \\ &= -\frac{\partial}{\partial x}(\mathbf{q}_{l1} \cdot \mathbf{e}_x) - ik\mathbf{q}_{l1} \cdot \mathbf{e}_y \end{aligned} \quad (5.15)$$

for the lower layer. Here, we take the basic state to be quasi-steady with respect to the lubrication front.

5.2. Local stability analysis: results

We locally approximate the basic state surface heights linearly near the lubrication front and summarise the resulting set of equations in the lubricated and unlubricated regions along with jump conditions in (E1)–(E9) of Appendix E. The method used to derive these local equations, valid in the vicinity of the lubrication front, follows that of the previous section on perturbations resisted dominantly by vertical shear. We solve these equations explicitly to obtain the dispersion relation in §E.0.2 and also perform an asymptotic analysis for large wavenumbers k . The asymptotics are outlined in §E.0.3 of

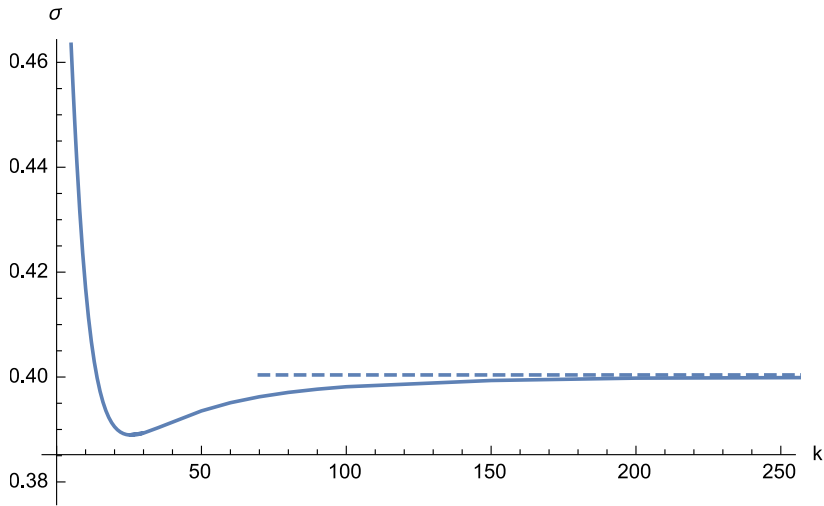


Figure 6: Asymptotic (dashed) and numerical (solid) solutions for the growth rates σ against wavenumber k for perturbations resisted dominantly by horizontal shear. Parameter values used are $\mathcal{M} = 10$ and $\mathcal{Q} = 0.1$.

Appendix E. The main message to take away can be captured concisely in the limit of $\mathcal{M} \rightarrow \infty$, in which the large- k behaviour of σ , is given by the simple relation

$$\sigma = \frac{\varphi_8 \mathcal{M}^2 + \varphi_9 \mathcal{M}}{\varphi_{10}} + \mathcal{O}(1/k, 1/\mathcal{M}), \quad (5.16)$$

where $\varphi_8, \dots, \varphi_{10}$ are functions of the basic state thicknesses, slopes and lubrication front velocity. Explicit expressions can be found in (S.113)–(S.115) of the Supplementary Material. The important message is that σ tends to a constant at large wavenumbers. This, in fact, is the case not only in the limit $\mathcal{M} \rightarrow \infty$, but holds for any value of \mathcal{M} and indicates that horizontal shear significantly stabilizes the flow at large wavenumber.

The large- k asymptotic solution for the growth rate σ is shown in Figure 6, where it is additionally seen that the full numerical solution of the equations, (E 1)–(E 9), described in Appendix E for the growth rate converges towards the asymptotic result.

This analysis reveals that horizontal shear provides a desirable stabilizing mechanism for large wavenumbers. In the following section, we wish to combine the physical ideas of §4 and the current section to determine the behaviour at intermediate wavenumbers.

6. Frontal dynamics: Intermediate regime for perturbations resisted by vertical and horizontal shear

In this section, we wish to consider the intermediate regime in which the flow of the basic state is resisted dominantly by vertical shear stresses while the flow of the perturbations is resisted dominantly by both vertical and horizontal shear stresses.

6.1. Model equations

6.1.1. Unlubricated region

With the lubrication approximation, the Stokes equations for the fluid flow in the unlubricated region are given by

$$0 = -\nabla p - \mathbf{e}_z + \left(\frac{\partial^2}{\partial y^2} + \frac{\partial^2}{\partial z^2} \right) \mathbf{u} \quad (6.1)$$

in dimensionless variables. A vertical balance of forces gives that the pressure is given hydrostatically by

$$p = H - z \quad (6.2)$$

whereas a horizontal balance gives

$$\nabla H = \left(\frac{\partial^2}{\partial y^2} + \frac{\partial^2}{\partial z^2} \right) \mathbf{u}. \quad (6.3)$$

To investigate the stability of the flow, we introduce small disturbances of size $\epsilon \ll 1$ and search for normal-mode solutions with transverse wavenumber k and growth rate σ of the form $X = X_0 + \epsilon X_1 + \dots$, where $X_1 = \hat{X}_1 \exp(iky + \sigma t)$ and $X = (H(x, y, t), \mathbf{u}(x, y, z, t), \mathbf{q}(x, y, t))$. The horizontal part of Stokes equations becomes

$$\frac{\partial H_0}{\partial x} \mathbf{e}_x + \epsilon \nabla H_1 = \frac{\partial^2 u_0}{\partial z^2} \mathbf{e}_x + \epsilon \left(-k^2 + \frac{\partial^2}{\partial z^2} \right) \mathbf{u}_1, \quad (6.4)$$

which has the following contribution at $\mathcal{O}(\epsilon)$

$$\nabla H_1 = \left(-k^2 + \frac{\partial^2}{\partial z^2} \right) \mathbf{u}_1. \quad (6.5)$$

For intermediate wavenumbers k , the effect of both horizontal and vertical shear stresses can become important and we retain both in the governing equations. The perturbed velocity is therefore exponential in z and resolve the boundary layers that were previously neglected in the limit in which horizontal shear was dominant. The full details are given in (F 1)–(F 2) of Appendix F, where the perturbed velocities and fluxes are given explicitly along with the mass conservation equations. We further apply local approximations valid in the vicinity of the lubrication front and match to the outer regions through decay conditions. This enables us to search for normal-mode solutions. The approach follows that of the previous two sections.

6.2. Lubricated region

Linearising the Stokes equations and looking for normal-mode solutions, while keeping the terms arising from both vertical and horizontal shear stresses, gives the following horizontal part of Stokes equations

$$\nabla H_0 + \epsilon \nabla H_1 = \frac{\partial^2 u_0}{\partial z^2} \mathbf{e}_x + \epsilon \left(\frac{\partial^2}{\partial y^2} + \frac{\partial^2}{\partial z^2} \right) \mathbf{u}_1, \quad (6.6)$$

$$\mathcal{M}(\nabla H_0 + \epsilon \nabla H_1) = \frac{\partial^2 u_{l0}}{\partial z^2} \mathbf{e}_x + \epsilon \left(\frac{\partial^2}{\partial y^2} + \frac{\partial^2}{\partial z^2} \right) \mathbf{u}_{l1}, \quad (6.7)$$

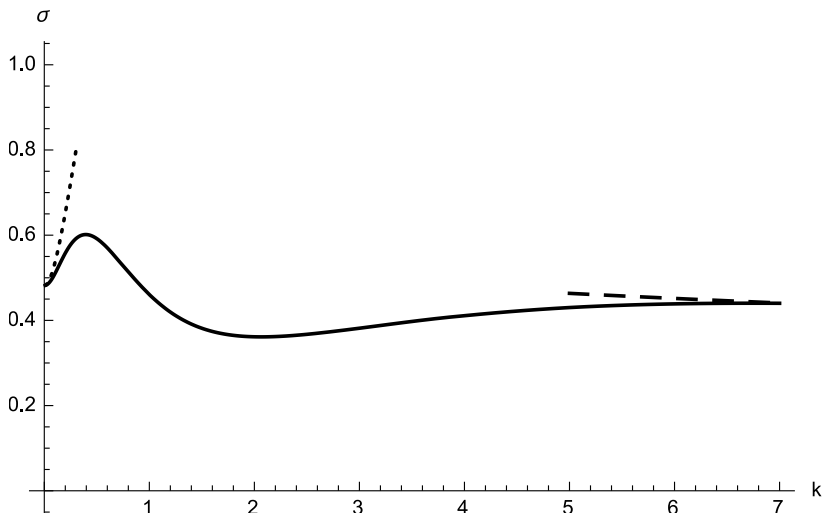


Figure 7: Growth rates σ against wavenumber k for perturbations resisted by vertical shear only (dotted), horizontal shear only (dashed), and both vertical and horizontal shear (solid). This figure uses results presented in figure 6 (dashed) for $k \gg 1$. Parameter values used are $\mathcal{M} = 10$ and $\mathcal{Q} = 0.1$.

for the two layers. This yields the following $\mathcal{O}(\epsilon)$ contributions

$$\nabla H_1 = \left(\frac{\partial^2}{\partial y^2} + \frac{\partial^2}{\partial z^2} \right) \mathbf{u}_1, \quad (6.8)$$

$$\mathcal{M} \nabla H_1 = \left(\frac{\partial^2}{\partial y^2} + \frac{\partial^2}{\partial z^2} \right) \mathbf{u}_{11}, \quad (6.9)$$

for the two layers. As the perturbations to the flow are resisted by both vertical and horizontal shear stresses, the gradients in z are comparable to the gradients in y . We, therefore, retain both and by looking for normal-mode solutions, obtain the following equations for the horizontal velocity

$$\nabla H_1 = \left(-k^2 + \frac{\partial^2}{\partial z^2} \right) \mathbf{u}_1 \quad (6.10)$$

for the upper layer and

$$\nabla H_1 = \left(-k^2 + \frac{\partial^2}{\partial z^2} \right) \mathbf{u}_{11} \quad (6.11)$$

for the lower layer. This approach resolves the small boundary layer at the interface between the two fluids and at the base, in which vertical shear stresses are important. The limit $kh \rightarrow \infty$ simplifies the problem to that of the previous section, in which horizontal shear stresses provide the dominant resistance to the flow of the perturbations and in which the effect of this boundary layer is negligible in a depth-averaged description of the flow.

6.3. Local stability analysis: results

Due to the terms proportional to $-k^2$, the horizontal velocities are given in terms of exponentials in z (in a finite domain) and present difficulties in obtaining a concise lubrication model. The reader is referred to Appendix F, specifically (F 1)–(F 2) and

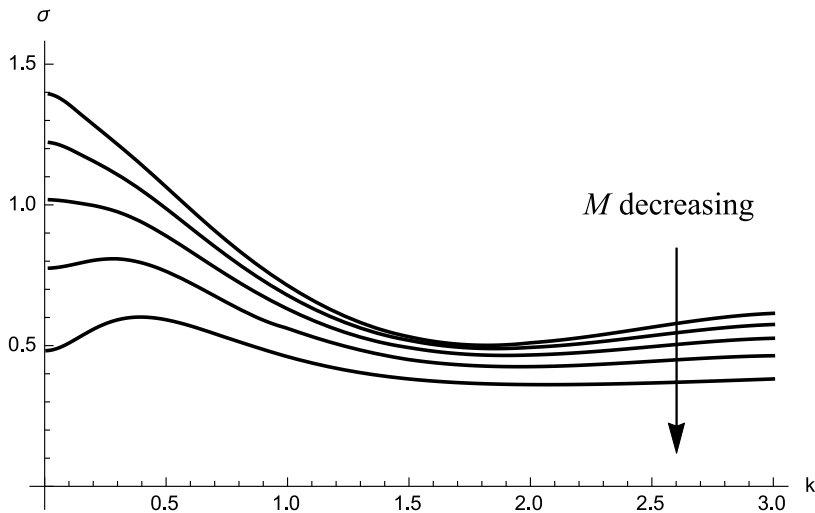


Figure 8: Growth rates σ against wavenumber k for perturbations resisted by both vertical and horizontal shear. Parameter values used are $\mathcal{M} = 10, 15, 20, 25, 30$ and $\mathcal{Q} = 0.1$.

(F 7)–(F 10), where the details of the derivation of the model, as well as the application of the local approximation and matching to the outer regions can be found.

Figure 7 shows the growth rates σ as a function of the transverse wavenumber k for representative parameter values, for the intermediate regime, considered in this section, in which the perturbations are resisted by both vertical and horizontal shear. Figure 7 also displays the growth rates for the small wavenumber limit in which vertical shear provides the dominant resistance to the flow of the perturbations and also the large wavenumber limit in which horizontal shear provides the dominant resistance to the flow of the perturbations. The intermediate regime, involving both vertical and horizontal shear stresses, is seen to converge to these small and large wavenumber limits in Figure 7.

Apart from the large-wavenumber stabilization analysed in the previous section, horizontal shear also stabilizes the flow at small wavenumbers. Figure 8 shows representative growth rates as a function of the wavenumber, for the intermediate regime, involving both vertical and horizontal shear stresses, for varying viscosity ratios \mathcal{M} . It is seen that small wavenumbers are the most unstable, and that the band of most unstable wavenumbers shifts towards smaller wavenumbers as the viscosity ratio increases. This does not necessarily imply that $k = 0$ is the most unstable wavenumber for these viscosity ratios, as a non-local analysis, valid for small wavenumbers, would be necessary to examine this.

7. Conclusions

We have carried out linear stability analyses of lubricated viscous gravity currents in two scenarios to isolate two different mechanisms of instability: internal and frontal. The former analysis shows that steady flow with no internal front is unconditionally stable and suggests that the instability observed in experiments is a frontal instability. The latter analysis explained the mechanism of instability by exploring three physical scenarios.

The first scenario occurs for wavelengths much larger than the thicknesses of the two

layers. We highlighted the underlying physical mechanism that drives the instability by using a combination of asymptotic and numerical methods. Analytically, we derived an asymptotic solution for the growth rate of the perturbations as an outer, large-wavenumber limit, which shows that the growth rate σ of the perturbations grows linearly with the wavenumber k as $k \rightarrow \infty$ with a prefactor that depends on the two layer thicknesses, the viscosity ratio as well as, crucially, the jump in upper surface slope, or hydrostatic pressure gradient, across the lubrication front. The latter ingredient, importantly, determines the sign of σ , that is, it determines whether or not the flow is unstable. By balancing upstream and downstream upper-layer fluxes, we further showed that this jump in upper surface slope is positive (that is, the flow is stable) precisely when the viscosity ratio \mathcal{M} between the two layers is less than one. That is, when a less viscous fluid lubricates a more viscous fluid – the setting relevant to our experiments and of geophysical interest – then the lubrication front is unstable; whereas if the situation is reversed and a more viscous fluid is injected underneath a less viscous fluid, then the flow remains stable.

The underlying instability mechanism involves a jump in *hydrostatic* pressure gradient across the lubrication front in contrast to Saffman-Taylor fingering, which occurs as a result of a jump in *dynamic* pressure gradient across the intrusion front. The instability mechanism can be understood physically by considering the lubrication front in the case in which a less viscous fluid intrudes beneath a more viscous fluid. If the lubrication front is perturbed so that the underlying, less viscous fluid dislocates to the no-slip region, then it becomes subject to higher hydrostatic pressure gradients and advances forward, feeding the instability. In the opposite case in which a more viscous fluid intrudes underneath a less viscous fluid, then if the front is perturbed so that the underlying, more viscous fluid dislocates to the no-slip region, then it becomes subject to lower hydrostatic pressure gradients and slows down, suppressing the instability.

By using a combination of asymptotic and numerical methods, we found that for the second scenario, involving perturbations resisted dominantly by horizontal shear stresses, the growth rate of the perturbations converges towards a constant rather than growing unboundedly. Transverse shear, therefore, provides an effective but weak stabilising mechanism at large wavenumbers. By considering the third, intermediate regime and formulating a fuller theoretical model accounting for both vertical and transverse shear stresses and solving it numerically, we found that transverse shear is weakly stabilizing for intermediate wavenumbers as well and that intermediate wavenumbers are the most unstable at modest values of \mathcal{M} . For larger values of \mathcal{M} , long waves are selected. In the companion paper, we consider effects of buoyancy and find further stabilization at long wavelengths.

KNK acknowledges the support of a NERC PhD studentship.

Supplementary Material Full expressions for coefficients used within this paper can be found in the Supplementary Material.

Appendix A. Tensorial form for lubricated currents with drainage

The prefactors a, A depend on the dimensionless parameters via

$$\frac{1}{4} \left[\frac{\mathcal{M}}{3} a^3 (\mathcal{D}a + A) + \frac{\mathcal{M}}{2} a^2 A (A - a) \right] = \mathcal{Q}, \quad (\text{A } 1)$$

$$\frac{1}{4} \left[\frac{1}{3}(A-a)^3 A + \frac{\mathcal{M}}{2} a^2 (A-a) (\mathcal{D}a + A) + \mathcal{M}aA(A-a)^2 \right] = 1. \quad (\text{A } 2)$$

The entries of \mathbf{C} are given by

$$C_{11} = 1, \quad C_{12} = 0, \quad C_{21} = -1, \quad C_{22} = 1, \quad (\text{A } 3)$$

the entries of \mathbf{E} are given by

$$\begin{aligned} E_{11} &= \frac{\mathcal{M}\mathcal{D}}{3} a^3, \\ E_{12} &= \frac{\mathcal{M}}{3} a^3 + \frac{\mathcal{M}}{2} a^2 (A-a), \\ E_{21} &= \frac{\mathcal{M}\mathcal{D}}{2} a^2 (A-a), \\ E_{22} &= \frac{1}{3} (A-a)^3 + \frac{\mathcal{M}}{2} a^2 (A-a) + \mathcal{M}a(A-a)^2, \end{aligned} \quad (\text{A } 4)$$

and the entries of \mathbf{F} are given by

$$\left\{ \begin{array}{l} F_{11} = \mathcal{M}a^2(\mathcal{D}a + A) + \frac{\mathcal{M}}{2}(-a^2A + 2aA(A-a)), \\ F_{12} = \frac{\mathcal{M}}{2}a^2A, \\ F_{21} = -(A-a)^2A + \frac{\mathcal{M}}{2}(2a(A-a) - a^2)(\mathcal{D}a + A) \\ \quad + \mathcal{M}((A-a)^2 - 2a(A-a))A, \\ F_{22} = (A-a)^2A + \frac{\mathcal{M}}{2}a^2(\mathcal{D}a + A) + 2\mathcal{M}a(A-a)A. \end{array} \right. \quad (\text{A } 5)$$

Appendix B. Second asymptotic solution near the drainage front

We wish to show that the leading order asymptotic solution is of the form

$$\mathbf{v}_0 \sim \zeta^{1/4} \mathbf{A}_0, \quad \text{as } \zeta \rightarrow 0 \quad (\text{B } 1)$$

where $\mathbf{A}_0 \in \mathbb{R}^2$ is a constant vector. As the the general solution to the leading order equation (3.12) in an inner region about the singular drainage front is

$$\mathbf{v}_0 = \zeta^{1/4} \mathbf{A}_0 + \zeta^{-M} \mathbf{B}_0, \quad (\text{B } 2)$$

it suffices to show that \mathbf{M} is positive definite for all parameter values, as in that case it is necessary that $\mathbf{B}_0 = \mathbf{0}$ to ensure that the zero-thickness boundary condition (3.8b) holds. After some algebra, it is possible to show that

$$\begin{aligned} \det(\mathbf{M}) &= \left[9(a^2\mathcal{D} + A^2) \left(a\mathcal{M}(a^2\mathcal{D} + 2A(A-a) + A^2) + \right. \right. \\ &\quad \left. \left. 2A(a-A)^2 \right) \right] \left[8a^2\mathcal{D}(a-A)^2 \left(3\mathcal{M}a + 4(A-a) \right) \right]^{-1} \\ &> 0. \end{aligned} \quad (\text{B } 3)$$

The positivity follows since each of the terms in the above quotient are positive, and the strict inequality follows since a and A are not both zero. After further algebra, it is also

possible to show that

$$\begin{aligned} \text{trace}(\mathbf{M}) &= \left[12(a-A)^2(A^3 + a^2(A-a)\mathcal{D} + a^2AD) + 3a(4(A-a)A^3 + \right. \\ &\quad \left. 2A^4 + 10\mathcal{D}a^2A(A-a) + a^2A^2\mathcal{D} + a^4\mathcal{D}(3+2\mathcal{D}))\mathcal{M} \right] \\ &\quad \left[4a^2(a-A)^2\mathcal{D}(4(A-a) + 3\mathcal{M}a) \right]^{-1} > 0. \end{aligned} \quad (\text{B4})$$

As before, the positivity follows since each of the terms in the above quotient are positive, and the strict inequality follows since a and A are not both zero. Therefore, since both the determinant and the trace of \mathbf{M} are strictly positive, then \mathbf{M} is positive definite, and this shows the claim holds.

Appendix C. Integral terms in dispersion relation

In order to show that the dispersion relation (3.17) yields only negative growth rates, it is sufficient to show that the integral terms in the dispersion relation are positive. To show this, it is sufficient to demonstrate that $\mathbf{J}^\dagger \mathbf{C}$ and $\mathbf{J}^\dagger \mathbf{E}$, are both positive definite, or equivalently, that $\tilde{\mathbf{J}}^\dagger \tilde{\mathbf{C}}$ and $\tilde{\mathbf{J}}^\dagger \tilde{\mathbf{E}}$ are positive definite where $\tilde{\mathbf{C}}$, $\tilde{\mathbf{E}}$, and $\tilde{\mathbf{J}}$ are given by (3.9). The equivalence follows since \mathbf{T} is invertable. The components of $\tilde{\mathbf{J}}$ are given by

$$\tilde{J}_{11} = \frac{1}{6}\mathcal{M}a(2aA + 6A^2 + a(A-a) + 8\mathcal{D}a^2) > 0, \quad (\text{C1})$$

$$\tilde{J}_{12} = 1/6\mathcal{M}a^2((A-a) + 5A) > 0, \quad (\text{C2})$$

$$\begin{aligned} \tilde{J}_{21} &= \frac{1}{6}(A-a)(2(A-a)^2 + 3\mathcal{M}a(A-a) + 3\mathcal{M}aA + \\ &\quad 6\mathcal{M}A^2 + 9\mathcal{M}\mathcal{D}a^2) > 0, \end{aligned} \quad (\text{C3})$$

$$\begin{aligned} \tilde{J}_{22} &= \frac{1}{6}(2((A-a) + 3A)(a-A)^2 + \\ &\quad 3a(6A(A-a) + a^2(1+\mathcal{D}))\mathcal{M}) > 0. \end{aligned} \quad (\text{C4})$$

The strict positivity follows since each of the terms above are strictly positive. This is because $A > a$, $a > 0$ and $A > 0$. Therefore, it follows that $\text{trace}(\tilde{\mathbf{J}}) > 0$. After some algebra, it is also possible to show that

$$\begin{aligned} \det(\tilde{\mathbf{J}}) &= \frac{1}{9}a\mathcal{M}(4(A-a)^2(3A^3 + \mathcal{D}a^2(A-a) + 3a^2AD) + \\ &\quad 3a\mathcal{M}(4A^3(A-a) + 2A^4 + a^2(3A-a)^2\mathcal{D} + 2a^4\mathcal{D}^2)) > 0 \end{aligned} \quad (\text{C5})$$

The strict positivity follows since the above is a sum of strictly positive terms as $A > a$, $a > 0$ and $A > 0$, as before. Therefore, $\tilde{\mathbf{J}}$ is positive definite, since its trace and determinant are strictly positive.

The components of $\tilde{\mathbf{E}}$ are given by

$$\tilde{E}_{11} = \frac{1}{6}a^2\mathcal{M}(2(A + \mathcal{D}a) + (A - a)) > 0, \quad (\text{C6})$$

$$\tilde{E}_{12} = \frac{1}{6}a^2\mathcal{M}((A - a) + 2A) > 0, \quad (\text{C7})$$

$$\tilde{E}_{21} = \frac{1}{6}\left(2(A - a)^3 + 3\mathcal{M}a(A - a)(A + (A - a) + \mathcal{D}a)\right) > 0, \quad (\text{C8})$$

$$\tilde{E}_{22} = \frac{1}{6}\left(2(A - a)^3 + 3a\mathcal{M}((A - a) + A)(A - a)\right) > 0. \quad (\text{C9})$$

The strict inequalities follow since the above entries are sums of positive terms. It follows from this that the trace of $\tilde{\mathbf{E}}$ is strictly positive. It is also possible to show that the determinant of $\tilde{\mathbf{E}}$ reduces to

$$\det(\tilde{\mathbf{E}}) = \frac{1}{36}\mathcal{M}\mathcal{D}a^3(A - a)^2(4(A - a) + 3\mathcal{M}a) > 0, \quad (\text{C10})$$

where the strict inequality follows from similar arguments as before. Therefore, since both the trace and the determinant of $\tilde{\mathbf{E}}$ are strictly positive, then $\tilde{\mathbf{E}}$ must be positive definite.

Since all the entries of $\tilde{\mathbf{J}}$ and $\tilde{\mathbf{E}}$ are strictly positive, then the trace of $\tilde{\mathbf{J}}^\dagger\tilde{\mathbf{E}}$ must also be strictly positive. Also note that $\det(\tilde{\mathbf{J}}^\dagger\tilde{\mathbf{E}}) = \det(\tilde{\mathbf{J}})\det(\tilde{\mathbf{E}}) > 0$. Therefore, $\tilde{\mathbf{J}}^\dagger\tilde{\mathbf{E}}$ is positive definite. The positive definitiveness of $\tilde{\mathbf{J}}^\dagger\tilde{\mathbf{C}}$ follows trivially since $\tilde{\mathbf{C}} = \mathbf{C}\mathbf{T} = \mathbf{I}$ is the identity matrix.

Appendix D. Derivation of local equations for perturbations resisted dominantly by vertical shear

For large enough wavenumbers k , the perturbations are localised near the lubrication front. Approximating the basic state linearly, that is, to first order in δ , near the front reduces the mass conservation equations (4.18)–(4.20) to

$$\begin{aligned} \sigma h_1 - Vh'_1 &= \left[b_{11}h_1 + (b_{12} + b_{13}k^2)H_1 + b_{14}h'_1 + b_{15}H'_1 + b_{16}H''_1 \right] + \\ &+ (x - x_{L0})e_{l1} + \mathcal{O}(x - x_{L0})^2 \quad (x \leq x_{L0}), \end{aligned} \quad (\text{D1})$$

$$\begin{aligned} \sigma H_1 - VH'_1 &= \left[b_1h_1 + (b_2 + b_3k^2)H_1 + b_4H'_1 + b_5H''_1 + b_6h'_1 \right] + \\ &+ (x - x_{L0})e_1 + \mathcal{O}(x - x_{L0})^2 \quad (x \leq x_{L0}) \end{aligned} \quad (\text{D2})$$

for the lubricated region and

$$\begin{aligned} \sigma H_1 - VH'_1 &= (2\alpha\beta^2 - \frac{1}{3}\alpha^3k^2)H_1 + 2\alpha^2\beta H'_1 + \frac{1}{3}\alpha^3H''_1 + (x - x_{L0})e_2 \\ &+ \mathcal{O}(x - x_{L0})^2 \quad (x \geq x_{L0}) \end{aligned} \quad (\text{D3})$$

for the unlubricated region. Here, b_{li}, b_i , for $i = 1, \dots, 6$, are functions of the basic state thicknesses a, A , slopes b, B and the viscosity ratio \mathcal{M} , whereas e_1, e_{l1}, e_2 are additionally functions of the perturbed quantities h_1, H_1 and their derivatives, and are listed in (S.7)–(S.21) of the Supplementary Material. Writing $x - x_L = \mathcal{O}(\delta)$, the mass conservation equations locally reduce to the zeroth order (in δ) balance of (D1)–(D3).

The first-order flux continuity boundary condition

$$\left\{ c_1 x_{L1} + \left[c_2 H_1 + c_3 h_1 + c_4 \frac{\partial H_1}{\partial x} \right] \right\}^- = \left\{ c_5 x_{L1} + \left[c_6 H_1 + c_7 \frac{\partial H_1}{\partial x} \right] \right\}^+ \quad (\text{D } 4)$$

consists of contributions from flux perturbations as well as from perturbations to the frontal position. Here, c_1, \dots, c_7 are functions of the basic state thicknesses h_0, H_0 and their gradients, as well as \mathcal{M} , and are given in (S.36)–(S.42) of the Supplementary Material. All quantities are to be evaluated at $x = x_{L0}$ from the side of the lubricated and unlubricated regions as indicated.

Appendix E. Derivation of local equations for perturbations resisted dominantly by horizontal shear

Near the lubrication front, we locally approximate the basic state surface heights linearly and find that the governing equation for the upper layer in the lubricated region becomes

$$\sigma(H_1 - h_1) - V(H'_1 - h'_1) = \xi_1 H_1 + \xi_2 H'_1 + \xi_3 H''_1 + \xi_4 h_1 + \xi_5 h'_1, \quad (\text{E } 1)$$

and for the lower layer,

$$\sigma h_1 - V h'_1 = \xi_6 H_1 + \xi_7 H'_1 + \xi_8 H''_1 + \xi_9 h_1 + \xi_{10} h'_1, \quad (\text{E } 2)$$

where ξ_1, \dots, ξ_{10} are given in (S.78)–(S.87) of the Supplementary Material.

After approximating the basic state surface heights linearly in the unlubricated region, the governing equation reduces to

$$\sigma H_1 - V H'_1 = \left(\frac{1}{2} \alpha^2 \beta H'_1 + \alpha \beta^2 H_1 - \alpha H_1 + \frac{1}{k^2} (\alpha H''_1 + \beta H'_1) \right) + \mathcal{O}(\beta(x - x_{L0})). \quad (\text{E } 3)$$

With the local approximation near the front, this further reduces to the zeroth order form, in $x - x_{L0}$, of the above.

E.0.1. Lubrication front

The condition (4.11) of continuity of flux across the lubrication front is given in terms of the perturbation to the combined flux of fluid in the x -direction in the lubricated region, which can be written as

$$\begin{aligned} (\mathbf{q}_1 + \mathbf{q}_{11}) \cdot \mathbf{e}_x &= \frac{1}{2} H_1 H'_0 \left(h_0^2 (\mathcal{M} - 1) - 2h_0 H_0 (\mathcal{M} - 1) - H_0^2 \right) \\ &\quad - \frac{1}{k^2} H'_1 \left(h_0 (\mathcal{M} - 1) + H_0 \right), \end{aligned} \quad (\text{E } 4)$$

by using the expressions (5.12)–(5.13). Using this and the expression (5.5) for the perturbation to the flux of fluid in the unlubricated region, we find that the flux condition becomes

$$\begin{aligned} &\left[\frac{1}{2} \left(H_1 H'_0 \left(h_0^2 (\mathcal{M} - 1) - 2h_0 H_0 (\mathcal{M} - 1) - H_0^2 \right) \right. \right. \\ &\quad \left. \left. - \frac{2}{k^2} H'_1 \left(h_0 (\mathcal{M} - 1) + H_0 \right) \right) + x_{L1} \frac{\partial}{\partial x} (\mathbf{q}_0 + \mathbf{q}_{10}) \cdot \mathbf{e}_x \right]^- \\ &= \left[-\frac{1}{2} \left(H'_0 H_0^2 H_1 + \frac{2}{k^2} H_0 H'_1 \right) + x_{L1} \frac{\partial}{\partial x} (\mathbf{q}_0 \cdot \mathbf{e}_x) \right]^+ \end{aligned} \quad (\text{E } 5)$$

By using the zeroth-order balance of the mass conservation equations to substitute for the basic state fluxes and using the local approximation near the front to linearise the basic state surface heights, we find that the flux condition becomes

$$\begin{aligned} & \left[\frac{1}{2} B H_1 \left(a^2 (\mathcal{M} - 1) - 2aA(\mathcal{M} - 1) - A^2 \right) - \frac{1}{k^2} H_1' \left(a(\mathcal{M} - 1) + A \right) \right]^- \\ & x_{L1} \left((-a^2 b B + a^2 B^2 + 2aAbB - 2aAB^2 - A^2 b B) (\mathcal{M} - 1) - A^2 B^2 \right) = \\ & - \frac{1}{2} \left[\beta \alpha^2 H_1 + \frac{2}{k^2} \alpha H_1' \right]^+ - \alpha^2 \beta^2 x_{L1} \end{aligned} \quad (\text{E } 6)$$

for $x = x_{L0}$. The condition of continuity of height gives

$$B x_{L1} + H_1^- = \beta x_{L1} + H_1^+ \quad (\text{E } 7)$$

for $x = x_{L0}$. The kinematic condition gives

$$\begin{aligned} \sigma x_{L1} = & \frac{1}{h_0^2} \left[\left(-x_{L1} h_0' \mathbf{q}_{10} \cdot \mathbf{e}_x + h_0 x_{L1} \frac{\partial}{\partial x} \mathbf{q}_{10} \cdot \mathbf{e}_x - h_1 \mathbf{q}_{10} \cdot \mathbf{e}_x \right) \right. \\ & + \frac{1}{2} \left(h_0^3 (H_1 - h_1) \mathcal{M} H_0' - h_0^3 H_1 H_0' - 2h_0^2 H_0 (H_1 - h_1) \mathcal{M} H_0' \right. \\ & \left. \left. + 2h_0^2 H_0 H_1 H_0' - h_0 H_0^2 H_1 H_0' - \frac{2}{k^2} h_0 (H_0 - h_0) H_1' \right) \right] \end{aligned} \quad (\text{E } 8)$$

for $x = x_{L0}^-$. Using zeroth order balances, we substitute for the basic state flux, apply the linear approximation for the surface heights near the front and find the local kinematic condition

$$\begin{aligned} \sigma x_{L1} = & \frac{1}{6a^2} \left[\left(3a^2 \mathcal{M} (-2ab + 3aB + 3Ab - 4AB) + 2(a - A)^2 (2ab \right. \right. \\ & \left. \left. - 3aB + Ab) \right) B x_{L1} + \left(\left(-3aA \mathcal{M} (a - 2A) - 2(a - A)^3 \right) B h_1 \right. \right. \\ & \left. \left. + 3 \left(a \mathcal{M} (a - 2A) - (a - A)^2 \right) a B H_1 \right) + \frac{6}{k^2} a (a - A) H_1' \right] \end{aligned} \quad (\text{E } 9)$$

for $x = x_{L0}^-$.

E.0.2. Dispersion relation

The mass conservation equations (E 3), (E 1)–(E 2) along with the height, flux and kinematic conditions (E 6)–(E 7), (E 9) form a system of linear differential equations with solutions

$$\begin{aligned} (h_1, H_1) &= (\tilde{h}_1^-, \tilde{H}_1^-) \exp((x - x_{L0})\lambda^-) \quad (x \leq x_{L0}), \\ H_1 &= \tilde{H}_1^+ \exp((x - x_{L0})\lambda^+) \quad (x \geq x_{L0}) \end{aligned} \quad (\text{E } 10a, b)$$

where $\tilde{h}_1^-, \tilde{H}_1^-, \tilde{H}_1^+$ are constants, after nondimensionalising by using the length and time scales found in (2.2). Direct substitution into the dimensionless versions of the mass conservation equations (E 3), (E 1)–(E 2) and boundary conditions (E 6)–(E 7), (E 9) gives the following governing equation for the unlubricated region

$$\sigma - V\lambda^+ = \frac{1}{2} \alpha^2 \beta \lambda^+ + \alpha \beta^2 - \alpha + \frac{1}{k^2} \left(\alpha (\lambda^+)^2 + \beta \lambda^+ \right), \quad (\text{E } 11)$$

and for the upper layer of the lubricated region

$$(\sigma - V\lambda^-)(\tilde{H}_1^- - \tilde{h}_1^-) = \left(\chi_1 + \chi_2\lambda^-\right)\tilde{h}_1^- + \left(\chi_3 + \chi_4\lambda^- + \chi_5(\lambda^-)^2\right)\tilde{H}_1^-, \quad (\text{E } 12)$$

and lower layer of the lubricated region

$$(\sigma - V\lambda^-)\tilde{h}_1^- = \left(\chi_{l1} + \chi_{l2}\lambda^-\right)\tilde{h}_1^- + \left(\chi_{l3} + \chi_{l4}\lambda^- + \chi_{l5}(\lambda^-)^2\right)\tilde{H}_1^-. \quad (\text{E } 13)$$

where χ_1, \dots, χ_5 , and $\chi_{l1}, \dots, \chi_{l5}$ are given in (S.88)–(S.92) and (S.100)–(S.104) of the Supplementary Material.

The flux continuity condition gives

$$\chi_6\tilde{H}_1^- + \chi_7\lambda^-\tilde{H}_1^- + \chi_8x_{L1} = -\frac{1}{2}\left(\beta\alpha^2\tilde{H}_1^+ + \frac{2}{k^2}\alpha\lambda^+\tilde{H}_1^+\right) - \alpha^2\beta^2x_{L1}, \quad (\text{E } 14)$$

and height continuity gives

$$Bx_{L1} + \tilde{H}_1^- = \beta x_{L1} + \tilde{H}_1^+. \quad (\text{E } 15)$$

The kinematic condition becomes

$$\sigma x_{L1} = \chi_9\tilde{h}_1^- + \chi_{10}\tilde{H}_1^- + \chi_{11}\lambda^-\tilde{H}_1^- + \chi_{12}x_{L1}, \quad (\text{E } 16)$$

where χ_6, \dots, χ_{12} are given in (S.93)–(S.99) of the Supplementary Material.

The mass conservation equations (E 11), (E 12)–(E 13) and height, flux and kinematic conditions (E 14)–(E 15), (E 16) is a system of six equations for six unknown variables $\sigma, x_{L1}, \tilde{h}_1^-, \tilde{H}_1^+, \lambda^-, \lambda^+$, where, as before, we set $\tilde{H}_1^- \equiv 1$, without loss of generality. The choice of solutions is restricted to those that satisfy decay conditions away from the lubrication front, that is, it is required that $\lambda^- > 0$ and $\lambda^+ < 0$.

E.0.3. Large- k asymptotics

The mass conservation equations for the lubricated region can be written in matrix form

$$(\mathbf{P} - (\sigma - V\lambda^-)\mathbf{I})[\tilde{h}_1^-, \tilde{H}_1^-]^T = \mathbf{0} \quad (\text{E } 17)$$

where the entries of the matrix \mathbf{P} are

$$\begin{aligned} P_{11} &= \left(Ab - \frac{1}{2}a^2\lambda^- + a(B - b + A\lambda^-) \right) BM \\ P_{12} &= \left(\frac{1}{k^2} \left(b\lambda^- + a(\lambda^-)^2 \right) - a \right) \mathcal{M} \\ P_{21} &= 0 \\ P_{22} &= (a - A) - (A - a)bB + (A - a)B^2 - aM + (A - a)bBM \\ &\quad + aB^2M + \lambda^- \left(-\frac{1}{2}a^2B(M - 1) + aAB(M - 1) + \frac{1}{2}A^2B \right) \\ &\quad + \frac{1}{k^2} \left((A - a)(\lambda^-)^2 + (B - b)\lambda^- + b\lambda^-M + a(\lambda^-)^2M \right). \end{aligned} \quad (\text{E } 18)$$

For non-trivial solutions, it is necessary that

$$\det(\mathbf{P} - (\sigma - V\lambda^-)\mathbf{I}) = 0 \quad (\text{E } 19)$$

giving a cubic equation for λ^- . Expanding in series of $1/k$ for k large,

$$\begin{aligned}
 \sigma &= \sigma_1 + \sigma_2/k + \dots, \\
 \lambda^\pm &= \lambda_{-1}^\pm k^2 + \lambda_0^\pm k + \dots, \\
 \tilde{H}_1^\pm &= \tilde{H}_{10}^\pm k + \tilde{H}_{11}^\pm + \dots, \\
 \tilde{h}_1^- &= \tilde{h}_{11}^- + k^{-1}\tilde{h}_{12}^- + \dots, \\
 x_{L1} &= x_{L11} + k^{-1}x_{L12} + \dots,
 \end{aligned} \tag{E 20}$$

gives that the leading order behaviour of the root λ^- is

$$\lambda^- = \frac{-(a-A)^2 B + a(a-2A)BM - 2V}{2(A + a(\mathcal{M}-1))} k^2 + \mathcal{O}(k) \tag{E 21}$$

so that λ_{-1}^- can be read from the leading order term above. Here, we exclude solutions for which $\lambda^- < 0$. The relationship between \tilde{h}_1^- and \tilde{H}_1^- can be determined from the equation of mass conservation for the lower layer to be

$$\tilde{h}_1^- = \frac{a\mathcal{M}(-(a-A)^2 B + a(a-2A)BM - 2V)}{(A + a(\mathcal{M}-1))(a(a-2A)BM - 2V)} + \mathcal{O}(1/k) \tag{E 22}$$

so that \tilde{h}_{11}^- can be read from the leading order term above. Here, recall that $\tilde{H}_1^- = 1$, without loss of generality. By solving the mass conservation equation for the unlubricated region for λ^+ , excluding the positive root and expanding in series of $1/k$, we find the leading order behaviour of λ^+ to be

$$\lambda^+ = \frac{2(-\alpha\beta^2 + \alpha + \sigma_1)}{\alpha^2\beta + 2V} + \mathcal{O}(1/k), \tag{E 23}$$

which tends to a constant as $k \rightarrow \infty$. Expanding the kinematic condition in series of $1/k$ gives the leading order behaviour of x_{L1} to be

$$x_{L1} = \frac{\varphi_1 \tilde{H}_1^- + \varphi_2 \tilde{h}_1^-}{\varphi_3} + \mathcal{O}(1/k), \tag{E 24}$$

which depends on the relation between \tilde{h}_1^- and \tilde{H}_1^- , where the φ_i are given in (S.106)–(S.115) of the Supplementary Material. Using (E 22) to substitute for the value of \tilde{h}_1^- and expanding in series of $1/k$ gives the leading order behaviour for x_{L1} to be

$$x_{L1} = \frac{\varphi_4}{\varphi_5} + \mathcal{O}(1/k). \tag{E 25}$$

Therefore, x_{L1} tends to a constant as $k \rightarrow \infty$. Height continuity gives the value of \tilde{H}_1^+

$$\tilde{H}_1^+ = \tilde{H}_1^- + (B - \beta)x_{L1}. \tag{E 26}$$

Substituting this into the condition of flux continuity gives an alternative expression for x_{L1}

$$x_{L1} = \frac{\varphi_6}{\varphi_7} \tilde{H}_1^- + \mathcal{O}(1/k). \tag{E 27}$$

Comparing this with the previous expression (E 25) for x_{L1} gives an implicit dispersion relation for σ . The explicit dispersion relation for σ , in the large- k limit, involves over 300 terms and is not written here for conciseness. The large- k behaviour of σ , in the limit

of $M \rightarrow \infty$, is given by

$$\sigma = \frac{\varphi_8 \mathcal{M}^2 + \varphi_9 \mathcal{M}}{\varphi_{10}} + \mathcal{O}(1/k, 1/\mathcal{M}). \quad (\text{E } 28)$$

Appendix F. Derivation of local equations for perturbations resisted by horizontal and vertical shear

F.1. Unlubricated region

The perturbed velocity components in the x - and y -directions are given by

$$u_1 = \frac{2}{k^2} \sinh\left(\frac{kz}{2}\right) \operatorname{sech}(kH_0) \left[\frac{\partial H_1}{\partial x} \sinh\left(\frac{1}{2}k(z - 2H_0)\right) + k \cosh\left(\frac{kz}{2}\right) H_1 \frac{\partial H_0}{\partial x} \right] \quad (\text{F } 1)$$

$$v_1 = \frac{2i}{k} \sinh\left(\frac{kz}{2}\right) H_1 \operatorname{sech}(kH_0) \sinh\left(\frac{1}{2}k(z - 2H_0)\right) \quad (\text{F } 2)$$

The components of the perturbation to the volume flux, per unit width, given by (5.4), can be found to be given by

$$q_{u1} = \frac{1}{2k^3} \left[2 \left(\tanh(kH_0) - kH_0 \right) \frac{\partial H_1}{\partial x} - kH_1 \left(k^2 H_0^2 + 2 \operatorname{sech}(kH_0) + 2 \right) \frac{\partial H_0}{\partial x} \right], \quad (\text{F } 3)$$

and

$$q_{v1} = \frac{i}{k^2} \left(\tanh(kH_0) - kH_0 \right) H_1. \quad (\text{F } 4)$$

The mass conservation equation for perturbations at the next order in ϵ gives

$$\begin{aligned} \sigma H_1 - V \frac{\partial H_1}{\partial x} &= -\nabla \cdot \mathbf{q}_1 \\ &= -\frac{\partial}{\partial x} (\mathbf{q}_1 \cdot \mathbf{e}_x) - ik \mathbf{q}_1 \cdot \mathbf{e}_y. \end{aligned} \quad (\text{F } 5)$$

By nondimensionalising and approximating the basic state surface heights piecewise linearly by (4.15) and assuming that the changes in surface slope, $\delta \frac{\partial H_0}{\partial x}$ are small in the vicinity of the lubrication front, the mass conservation equation for the unlubricated region reduces to

$$\begin{aligned} \sigma H_1 - V \frac{\partial H_1}{\partial x} &= \left(\frac{1}{k} \tanh(\alpha k) (\beta^2 \operatorname{sech}(\alpha k) + 1) + \alpha (\beta^2 - 1) \right) H_1 \\ &+ \left(\frac{\beta (\alpha^2 k^2 + 4) - 2\beta \operatorname{sech}(\alpha k) (\operatorname{sech}(\alpha k) + 1) + 2k^2 \dot{x}_{L0}}{2k^2} \right) \frac{\partial H_1}{\partial x} \\ &+ \left(\frac{\alpha k - \tanh(\alpha k)}{k^3} \right) \frac{\partial^2 H_1}{\partial x^2}. \end{aligned} \quad (\text{F } 6)$$

F.2. Lubricated region

The x - and y -components of the perturbed velocity field in the upper layer may be written as

$$u_1 = \frac{1}{\alpha_1} \left(\gamma_1 h_1 + \gamma_2 H_1 + \gamma_3 \frac{\partial H_1}{\partial x} \right), \quad (\text{F } 7)$$

$$v_1 = i \frac{\gamma_4}{\alpha_1} H_1 \quad (\text{F } 8)$$

where the coefficients are given in (S.116)–(S.120) of the Supplementary Material.

The x - and y -components of the perturbed velocity field in the lower layer are

$$u_{l1} = \frac{1}{\alpha_1} \left(\gamma_{l1} h_1 + \gamma_{l2} H_1 + \gamma_{l3} \frac{\partial H_1}{\partial x} \right), \quad (\text{F } 9)$$

$$v_{l1} = i \frac{\gamma_{l4}}{\alpha_1} H_1 \quad (\text{F } 10)$$

where the γ_{li} are given in (S.121)–(S.124) of the Supplementary Material.

The components of the depth-integrated volume flux, per unit width, for the upper layer are

$$q_{u1} = \frac{1}{\alpha_1} \left(\gamma_{q1} h_1 + \gamma_{q2} H_1 + \gamma_{q3} \frac{\partial H_1}{\partial x} \right), \quad (\text{F } 11)$$

$$v_1 = i \frac{\gamma_{q4}}{\alpha_1} H_1 \quad (\text{F } 12)$$

where the γ_{qi} are given in (S.125)–(S.128) of the Supplementary Material.

Conservation of mass at first order in ϵ is given by

$$\begin{aligned} \sigma(H_1 - h_1) - V \frac{\partial(H_1 - h_1)}{\partial x} &= -\nabla \cdot \mathbf{q}_1 \\ &= -\frac{\partial}{\partial x} (\mathbf{q}_1 \cdot \mathbf{e}_x) - ik \mathbf{q}_1 \cdot \mathbf{e}_y \end{aligned} \quad (\text{F } 13)$$

for the upper layer and

$$\begin{aligned} \sigma h_1 - V \frac{\partial h_1}{\partial x} &= -\nabla \cdot \mathbf{q}_{l1} \\ &= -\frac{\partial}{\partial x} (\mathbf{q}_{l1} \cdot \mathbf{e}_x) - ik \mathbf{q}_{l1} \cdot \mathbf{e}_y \end{aligned} \quad (\text{F } 14)$$

for the lower layer.

In what follows, we approximate the basic state surface heights piecewise linearly by (4.15) and also assume that the changes in surface slope, $\delta \frac{\partial H_0}{\partial x}$ and $\delta \frac{\partial h_0}{\partial x}$, of the two layers are small in the vicinity of the lubrication front. After nondimensionalising, this reduces the mass conservation equation for the upper layer to

$$\sigma(H_1 - h_1) - V \frac{\partial(H_1 - h_1)}{\partial x} = \beta_1 h_1 + \beta_2 H_1 + \beta_3 \frac{\partial h_1}{\partial x} + \beta_4 \frac{\partial H_1}{\partial x} + \beta_5 \frac{\partial^2 H_1}{\partial x^2} \quad (\text{F } 15)$$

where the coefficients β_1, \dots, β_5 depend on the basic state thicknesses and surface slopes as well as the wavenumber and are given in (S.129)–(S.133) of the Supplementary Material. Similarly, the mass conservation equation for the lower layer reduces to

$$\sigma h_1 - V \frac{\partial h_1}{\partial x} = \beta_{l1} h_1 + \beta_{l2} H_1 + \beta_{l3} \frac{\partial h_1}{\partial x} + \beta_{l4} \frac{\partial H_1}{\partial x} + \beta_{l5} \frac{\partial^2 H_1}{\partial x^2}. \quad (\text{F } 16)$$

The coefficients $\beta_{l1}, \dots, \beta_{l5}$ are given in (S.135)–(S.139) of the Supplementary Material.

F.3. Lubrication front

The condition (4.11) of continuity of flux across the lubrication front gives

$$\left[\kappa_1 h_1 + \kappa_2 H_1 + \kappa_3 \frac{\partial H_1}{\partial x} + x_{L1} \left(\frac{\partial q_{u0}}{\partial x} + \frac{\partial q_{ul0}}{\partial x} \right) \right]^- = \quad (\text{F 17})$$

$$\left[\kappa_4 H_1 + \kappa_5 \frac{\partial H_1}{\partial x} + x_{L1} \frac{\partial q_{u0}}{\partial x} \right]^+, \quad (\text{F 18})$$

at $x = x_{L0}$, where the coefficients $\kappa_1, \dots, \kappa_5$ are given in terms of the basic state thicknesses and surface gradients at the lubrication front, and are specified in (S.140)–(S.144) of the Supplementary Material.

Continuity of height gives

$$\left[x_{L1} \frac{\partial H_0}{\partial x} + H_1 \right]^- = \left[x_{L1} \frac{\partial H_0}{\partial x} + H_1 \right]^+, \quad (\text{F 19})$$

at $x = x_{L0}$. The kinematic condition reduces to

$$\sigma x_{L1} = \kappa_6 h_1 + \kappa_7 H_1 + \kappa_8 \frac{\partial H_1}{\partial x} + \kappa_9 x_{L1}, \quad (\text{F 20})$$

at $x = x_{L0}$, where the coefficients $\kappa_6, \dots, \kappa_9$ depend on basic state thicknesses and surface gradients as well as on the basic state flux and its gradient at the lubrication front. The coefficients are specified in closed form in (S.145)–(S.148) of the Supplementary Material.

F.4. Dispersion relation

The three mass conservation equations form a fifth-order system of differential equations. Together with the height, flux and kinematic conditions as well as the two asymptotic decay conditions as $x \rightarrow \infty$ and as $x \rightarrow -\infty$, this forms a fully specified system of linear differential equations with general solutions given by (E 10) in terms of the amplitudes $\tilde{h}_1^-, \tilde{H}_1^-, \tilde{H}_1^+$.

Direct substitution into the mass conservation equations yields

$$\sigma(\tilde{H}_1^- - \tilde{h}_1^-) - V\lambda^-(\tilde{H}_1^- - \tilde{h}_1^-) = \beta_1 \tilde{h}_1^- + \beta_2 \tilde{H}_1^- + \beta_3 \lambda^- \tilde{h}_1^- + \beta_4 \lambda^- \tilde{H}_1^- + (\lambda^-)^2 \tilde{H}_1^-, \quad (\text{F 21})$$

for the upper layer and

$$\sigma \tilde{h}_1^- - V\lambda^- \tilde{h}_1^- = \beta_{11} \tilde{h}_1^- + \beta_{12} \tilde{H}_1^- + \beta_{13} \lambda^- \tilde{h}_1^- + \beta_{14} \lambda^- \tilde{H}_1^- + \beta_{15} (\lambda^-)^2 \tilde{H}_1^-, \quad (\text{F 22})$$

for the lower layer of the lubricated region and

$$\begin{aligned} \sigma - V\lambda^+ &= \left(\frac{1}{k} \tanh(\alpha k) (\beta^2 \text{sech}(\alpha k) + 1) + \alpha (\beta^2 - 1) \right) \\ &+ \left(\frac{\beta (\alpha^2 k^2 + 4) - 2\beta \text{sech}(\alpha k) (\text{sech}(\alpha k) + 1) + 2k^2 \dot{x}_{L0}}{2k^2} \right) \lambda^+ \\ &+ \left(\frac{\alpha k - \tanh(\alpha k)}{k^3} \right) (\lambda^+)^2 \end{aligned} \quad (\text{F 23})$$

for the unlubricated region. Continuity of flux gives

$$\kappa_1 \tilde{h}_1^- + \kappa_2 \tilde{H}_1^- + \kappa_3 \lambda^- \tilde{H}_1^- + x_{L1} \left(\frac{\partial q_{u0}^-}{\partial x} + \frac{\partial q_{ul0}^-}{\partial x} \right) = \quad (\text{F 24})$$

$$\kappa_4 \tilde{H}_1^+ + \kappa_5 \lambda^+ \tilde{H}_1^+ + x_{L1} \frac{\partial q_{u0}^+}{\partial x}, \quad (\text{F 25})$$

Continuity of height gives

$$x_{L1} \frac{\partial H_0^-}{\partial x} + \tilde{H}_1^- = x_{L1} \frac{\partial H_0^+}{\partial x} + \tilde{H}_1^+, \quad (\text{F } 26)$$

while the kinematic condition reduces to

$$\sigma x_{L1} = \kappa_6 \tilde{h}_1^- + \kappa_7 \tilde{H}_1^- + \kappa_8 \lambda^- \tilde{H}_1^- + \kappa_9 x_{L1}, \quad (\text{F } 27)$$

The above system of six algebraic equations can be solved for the six unknowns x_{L1} , \tilde{h}_1^- , \tilde{H}_1^+ , λ^- , λ^+ and σ , where, as before, $H_1^- \equiv 1$, without loss of generality.

REFERENCES

- AL-HOUSSEINY, T. T., TSAI, P. A. & STONE, H. A. 2012 Control of interfacial instabilities using flow geometry. *Nat. Phys.* **8**, 747.
- BALMFORTH, N. J. & CRASTER, R. V. 2000 Dynamics of cooling domes of viscoplastic fluid. *J. Fluid Mech.* **422**, 225–248.
- BALMFORTH, N. J., CRASTER, R. V. & TONIOLO, C. 2003 Interfacial instability in non-newtonian fluid layers. *Phys. Fluids*. **15** (11), 3370–3384.
- BEN-JACOB, E., GODBEY, R., GOLDENFELD, N. D., KOPLIK, J., LEVINE, H., MUELLER, T. & SANDER, L. M. 1985 Experimental demonstration of the role of anisotropy in interfacial pattern formation. *Phys. Rev. Lett.* **55**, 1892.
- CHEN, J. D. 1989 Growth of radial viscous fingers in a hele-shaw cell. *J. Fluid Mech.* **201**, 223–242.
- CHEN, K. P. 1993 Wave formation in the gravity driven low reynolds number flow of two liquid films down an inclined plane. *Phys. Fluids A* **5** (12), 3038–3048.
- CINAR, Y., RIAZ, A. & TCHELEPI, H. A. 2009 Experimental study of co2 injection into saline formations. *Soc. Petrol. Engrs J.* **14**, 589–594.
- DIAS, E. O., ALVAREZ-LACALLE, E., CARVALHO, M. S. & MIRANDA, J. A. 2012 Minimization of viscous fluid fingering: a variational scheme for optimal flow rates. *Phys. Rev. Lett.* **109**, 144502.
- DIAS, E. O. & MIRANDA, J. A. 2010 Control of radial fingering patterns: a weakly nonlinear approach. *Phys. Rev. E* **81**, 016312.
- DIAS, E. O. & MIRANDA, J. A. 2013 Taper-induced control of viscous fingering in variable-gap hele-shaw flows. *Phys. Rev. E* **87**, 053015.
- FAST, P., KONDIC, L., SHELLEY, M. J. & PALFFY-MUHORAY, P. 2001 Pattern formation in non-Newtonian Hele-Shaw flow. *Phys. Fluids* **13**, 1191–1212.
- FOWLER, A. C. & JOHNSON, C. 1995 Hydraulic run-away a mechanism for thermally regulated surges of ice sheets. *J. Glaciol.* **41** (139), 554–561.
- FOWLER, A. C. & JOHNSON, C. 1996 Ice sheet surging and ice stream formation. *Ann. Glaciol.* **23**, 68–73.
- HINCH, E. J. 1984 A note on the mechanism of the instability at the interface between two shearing fluids. *J. Fluid Mech.* **144**, 463–465.
- HINDMARSH, R. C. A. 2004 Thermoviscous stability of ice-sheet flows. *J. Fluid Mech.* **502**, 17–40.
- HINDMARSH, R. C. A. 2006 Stress gradient damping of thermoviscous ice flow instabilities. *J. Geophys. Res.* **111**.
- HOMSY, G. M. 1987 Viscous fingering in porous media. *Annu. Rev. Fluid Mech.* **19**, 271.
- HOOPER, A. P. 1989 The stability of two superposed viscous fluids in a channel. *Phys. Fluids A* **1** (7), 1133–1142.
- HOOPER, A. P. & BOYD, W. G. C. 1983 Shear-flow instability at the interface between two viscous fluids. *J. Fluid Mech.* **128**, 507–528.
- HOOPER, A. P. & BOYD, W. G. C. 1987 Shear-flow instability due to a wall and a viscosity discontinuity at the interface. *J. Fluid Mech.* **179**, 201–225.
- HOOPER, A. P. & GRIMSHAW, R. 1985 Nonlinear instability at the interface between two viscous fluids. *Phys. Fluids* **28** (1), 37–45.

- HUPPERT, H. E. 1982 The propagation of two-dimensional and axisymmetric viscous gravity currents over a rigid horizontal surface. *J. Fluid Mech.* **121**, 43–58.
- JUEL, A. 2012 Flattened fingers. *Nat. Phys.* **8**, 706–707.
- KAGEI, N., KANIE, D. & KAWAGUCHI, M. 2005 Viscous fingering in shear thickening silica suspensions. *Phys. Fluids* **17**, 054103.
- KAO, T. W. 1968 Role of viscosity stratification in the stability of two-layer flow down an incline. *J. Fluid Mech.* **33**, 561–572.
- KONDIC, L., SHElLEY, M. J. & PALFFY-MUHORAY, P. 1998 Non-newtonian hele-shaw flow and the saffman-taylor instability. *Phys. Rev. Lett.* **80**, 1433–1436.
- KOWAL, K. 2016 The fluid mechanics of lubricated ice sheets. PhD thesis, University of Cambridge.
- KOWAL, K. N. & WORSTER, M. G. 2015 Lubricated viscous gravity currents. *J. Fluid Mech.* **766**, 626–655.
- KOWAL, K. N. & WORSTER, M. G. 2018 Stability of lubricated viscous gravity currents. Part 2: Global analysis and stabilisation by buoyancy forces. *Submitted to J. Fluid Mech.*
- KYRKE-SMITH, T. M., KATZ, R. F. & FOWLER, A. C. 2014 Subglacial hydrology and the formation of ice streams. *Proc. R. Soc. A.* **470**, 20130494.
- LI, S., LOWENGRUB, J. S., FONTANA, J. & PALFFY-MUHORAY, P. 2009 Control of viscous fingering patterns in a radial hele-shaw cell. *Phys. Rev. Lett.* **102**, 174501.
- LOEWENHERZ, D. S. & LAWRENCE, C. J. 1989 The effect of viscosity stratification on the stability of a free surface flow at low reynolds number. *Phys. Fluids A* **1** (10), 1686–1693.
- LOEWENHERZ, D. S., LAWRENCE, C. J. & WEAVER, R. L. 1989 On the development of transverse ridges on rock glaciers. *J. Glaciol.* **35** (121), 383–391.
- MANICKAM, O. & HOMS, G. M. 1993 Stability of miscible displacements in porous media with nonmonotonic viscosity profiles. *Phys. Fluids A* **5** (6), 1356–1367.
- MULLINS, W. W. & SEKERKA, R. F. 1964 Stability of a planar interface during solidification of a dilute binary alloy. *J. Appl. Phys.* **35** (2), 444–451.
- NASE, J., DERKS, D. & LINDNER, A. 2011 Dynamic evolution of fingering patterns in a lifted hele-shaw cell. *Phys. Fluids* **23**, 123101.
- ORR, F. M. & TABER, J. J. 1984 Use of carbon dioxide in enhanced oil recovery. *Science* **224**, 563–569.
- PATERSON, L. 1981 Radial fingering in a hele-shaw cell. *J. Fluid Mech.* **113**, 513–529.
- PAYNE, A. J. & DONGELMANS, P. 1997 Self-organization in the thermo-mechanical flow of ice-sheets. *J. Geophys. Res.* **102** (B6), 12,219–12,233.
- PIHLER-PUZOVIC, D., ILLIEN, P., HEIL, M. & JUEL, A. 2012 Suppression of complex fingerlike patterns at the interface between air and a viscous fluid by elastic membranes. *Phys. Rev. Lett.* **108**, 074502.
- PIHLER-PUZOVIC, D., JUEL, A. & HEIL, M. 2014 The interaction between viscous fingering and wrinkling in elastic-walled hele-shaw cells. *Phys. Fluids* **26**, 022102.
- PIHLER-PUZOVIC, D., PERILLAT, R., RUSSELL, M., JUEL, A. & HEIL, M. 2013 Modelling the suppression of viscous fingering in elastic-walled hele-shaw cells. *J. Fluids Mech.* **731**, 161.
- REINELT, D. A. 1995 The primary and inverse instabilities of directional fingering. *J. Fluid Mech.* **285**, 303.
- RENARDY, Y. 1987 Viscosity and density stratification in vertical poiseuille flow. *Phys. Fluids* **30**, 1638–1648.
- SAFFMAN, P. G. & TAYLOR, G. 1958 The penetration of a fluid into a porous medium or Hele-Shaw cell containing a more viscous liquid. *Proc. R. Soc. Lond. A* **245**, 312–329.
- SAYAG, R. & TZIPERMAN, E. 2008 Spontaneous generation of pure ice streams via flow instability: Role of longitudinal shear stresses and subglacial till. *J. Geophys. Res.* **113**, b05411.
- SAYAG, R. & TZIPERMAN, E. 2009 Spatiotemporal dynamics of ice streams due to a triple-valued sliding law. *J. Fluid Mech.* **640**, 483–505.
- TAYLOR, G. I. 1963 Cavitation of a viscous fluid in narrow passages. *J. Fluid Mech.* **16**, 595–619.
- THOME, T., RABAUD, M., HAKIM, V. & COUDER, Y. 1989 The Saffman-Taylor instability: from the linear to the circular geometry. *Phys. Fluids A* **1**, 224–240.
- TILLEY, B. S., DAVIS, S. H. & BANKOFF, S. G. 1994 Linear stability theory of two-layer fluid flow in an inclined channel. *Phys. Fluids* **6** (12), 3906–3922.

- TONIOLO, C. 2001 Slipping instability in a system of two superposed fluid layers. In *Proceedings of the Geophysical Fluid Dynamics program*. Woods Hole Oceanographic Institution.
- WANG, C. K., SEABORG, J. J. & LIN, S. P. 1978 Instability of multilayered liquid films. *Phys. Fluids* **21** (10), 1669–1673.
- YIH, C. S. 1967 Instability due to viscosity stratification. *J. Fluid Mech.* **27**, 337–352.